NASA TN D-82

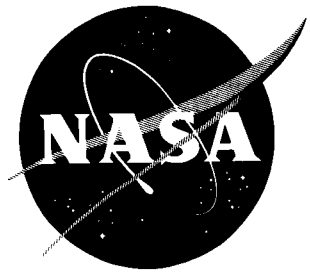

TECHNICAL NOTE

D-82

CONTROL OF COMBUSTION-CHAMBER PRESSURE AND OXIDANT-FUEL RATIO FOR A REGENERATIVELY COOLED HYDROGEN-FLUORINE ROCKET ENGINE

By Edward W. Otto and Richard A. Flage

Lewis Research Center
Cleveland, Ohio

NATIONAL AERONAUTICS AND SPACE ADMINISTRATION
WASHINGTON
November 1959

NATIONAL AERONAUTICS AND SPACE ADMINISTRATION

TECHNICAL NOTE D-82

CONTROL OF COMBUSTION-CHAMBER PRESSURE AND OXIDANT-FUEL RATIO FOR A REGENERATIVELY COOLED HYDROGEN-FLUORINE ROCKET ENGINE

By Edward W. Otto and Richard A. Flage

SUMMARY

The design of a chamber-pressure and mixture-ratio control system to increase the safety and speed of testing and to investigate the general controllability of a regeneratively cooled hydrogen-fluorine rocket engine is presented. The dynamics of the components of the system and of the complete control loop are investigated. Time-history records of combustion-chamber pressure and mixture ratio illustrating control-system performance are presented. The system proved capable of starting a hydrogen-fluorine rocket engine, providing stable operation to within ± 2 percent of the preset values of chamber pressure and mixture ratio, and limiting transient deviations in oxidant-fuel ratio sufficiently to avoid a stoichiometric mixture.

INTRODUCTION

A research program was undertaken at the NASA Lewis Research Center to investigate the performance and cooling requirements of a regeneratively cooled hydrogen-fluorine rocket engine. A chamber-pressure and oxidant-fuel-ratio control system was developed for this program in order to increase the safety during the experiments, to increase the amount of data obtained in a given amount of running time, and to investigate the general controllability of the engine and propellant combination. This control system contributed to the safety of the experiments by incorporating rapid shutoff valves and flow control of each propellant independent of engine operating conditions. Data were obtained at an increased rate because provision was made for running several engine operating conditions (P_c or O/F) consecutively.

Control of combustion-chamber pressure and oxidant-fuel ratio was used in this program, although the technique for control of thrust and oxidant-fuel ratio would be similar. The control-system analysis that

follows shows the control techniques employed and their effect on the selection of control components and presents an investigation of the dynamics of the components and the complete control-loop dynamics. A time-history record of combustion-chamber pressure and oxidant-fuel ratio illustrating control-system performance is presented; and the adequacy of dynamic response, steady-state and dynamic accuracy, and factors affecting these characteristics are discussed.

The tests in this report cover a range of oxidant-fuel ratio from 6.14 to 15.67 and chamber pressure from 300 to 60 pounds per square inch absolute.

APPARATUS

Figure 1 shows a schematic diagram of the rocket engine and propellant feed system. Each propellant was fed from a pressurized tank by means of a dip tube through a Venturi and control valve to the engine. The fluorine tank was stainless steel and was suspended in a liquid-nitrogen bath, and the lines, Venturi, and control valve were located in a trough filled with liquid nitrogen. The fluorine tank was pressurized with helium to a maximum working pressure of 1500 pounds per square inch. The hydrogen tank was stainless steel and constructed with first a vacuum jacket and then a surrounding liquid-nitrogen jacket. The line between the tank and engine was insulated with Styrofoam. The tank was pressurized with hydrogen gas to a maximum working pressure of 1500 pounds per square inch.

The fluorine Venturi was located approximately midway between the tank and the engine. The fluorine control valve was located approximately 2 feet downstream of the Venturi and about 3 feet upstream of the engine. The hydrogen Venturi was located at the bottom of the dip tube, and the control valve was located on the engine inlet. The total length of the hydrogen line between the Venturi and the control valve was approximately 25 feet.

The Venturi ΔP pickups were of the differential strain-gage type and were closely connected with tubing (1/16-in. I.D. for the hydrogen and 1/8-in. I.D. for the fluorine) to their respective Venturis. To minimize the length of the liquid column, the fluorine pickup lines were insulated from the liquid-nitrogen bath and electrically heated. The signals from the ΔP pickups were amplified to produce 1 volt for full-scale ΔP. The full-scale value of ΔP could be chosen by varying the gain of the amplifying equipment. The full-scale sensitivity of the ΔP pickup and the Venturi size could be chosen for best accuracy at the desired flow conditions.

Chamber pressure was measured with a strain-gage pressure pickup, and the resulting electrical signal was amplified to the 1-volt level for full-scale pressure. Thrust was measured with a strain-gage load cell, and the resulting electrical signal was amplified to the 1-volt level for full-scale thrust. The nominal chamber pressure was 300 pounds per square inch absolute, and the nominal thrust of this engine was 5000 pounds.

The control valve consisted of a standard plug valve body, seal, and linear plug and seat assembly actuated by a specially designed electro-hydraulic servovalve and piston assembly. This assembly, together with the valve-position pickup and the electronic amplifier, formed a positional servomotor by means of which the propellant control valve could be rapidly positioned in response to an input voltage.

E-211

CONTROL-SYSTEM ANALYSIS

Control Method

CF-1 back

The basic flow control loop for each propellant is shown in figure 2(a). In each case the loop was closed around flow by comparing the 0- to 1-volt ΔP signal with a desired voltage and feeding the resulting error voltage to the control-valve servomotor. In order to obtain oxidant-fuel-ratio control and combustion-chamber-pressure control, the basic flow systems were altered as shown in figure 2(b).

Oxidant-fuel ratio was obtained as shown in figure 2(b) by feeding the fuel and oxidant ΔP signals to opposite ends of a potentiometer and feeding the resulting signal at the wiper arm to the oxidant control-valve servomotor. The resulting valve movement varies oxidant flow until zero voltage is obtained at the wiper arm. This method of obtaining O/F control requires that the oxidant voltage be 0 to -1 volt for full-scale ΔP range. The desired O/F can be set by setting the position of the wiper arm.

Control of the chamber pressure was obtained by comparing the 0- to 1-volt P_c signal with a desired voltage and feeding the resulting error voltage to the fuel control-valve servomotor. The resulting valve movement varies fuel flow, which in turn varies oxidant flow. This change in propellant flows varies chamber pressure, and the control action continues until zero error voltage is obtained at the input of the fuel control-valve servomotor.

It is also possible to obtain O/F control by varying fuel flow, and P_c control by varying oxidant flow. However, the method shown was chosen because it more easily satisfies certain of the safety requirements. Specifically, it makes certain that there is no oxidant flow unless fuel

is actually flowing. It also lends itself to providing the fuel-flow lead necessary for purging of the engine and line cooling.

In order to avoid attack of uncombined fluorine on chamber walls, the engine must be run below the O/F corresponding to stoichiometric (approx. 19), or fuel-rich. With the control method chosen (i.e., control of O/F through oxidant flow and control of P_c through fuel flow), it was necessary to reduce deliberately the speed of response of the fuel control loop below the maximum permissible response speed of the oxidant control loop so that the oxidant-flow control could follow the most rapid variations in fuel flow. This technique ensures that transient deviations in O/F never go above stoichiometric.

System Component Dynamics

A block diagram of the P_c and O/F control system is presented in figure 3(a), which shows the various elements in the system and their interrelation. It is to be noticed that both the chamber-pressure control loop and the mixture-ratio control loop are affected by variations in oxidant and fuel flows. Figure 3(b) is a block diagram of the system indicating the approximate form of the dynamic response of each of the elements in the system, where the K terms are the steady-state values and the G terms denote the dynamic response (see appendix A). A controller with dynamic characteristics represented by G_O or G_{1O} has been added in each loop in order to make the loop representation as complete as possible. In order to solve for the complete loop dynamics, it is necessary to obtain the transfer function for each component shown in figure 3(b). These transfer functions were obtained as discussed in the following section. The necessary form of the transfer functions G_O and G_{1O} for most satisfactory loop dynamics and stability is determined in a later section. All the values for the K terms are presented in table I. The G terms are presented in curve form.

Servo-operated control valve. - The electrohydraulic actuator for each propellant control valve was designed to provide as high a speed of response as is reasonably attainable in order to reach operating conditions quickly and to satisfy the safety requirement that the control valve close rapidly upon signal. The construction of the actuator and of the associated equipment that form the positional servomotor is described in appendix B.

The frequency response of each control valve was determined by feeding an error signal from a signal generator to the input of the servoamplifier and measuring valve position response. The amplitude ratio of valve position to input voltage and the resulting phase lag were measured on an oscilloscope. The results of the frequency-response tests to inputs

corresponding to ±5, ±10, and ±20 percent of the total valve stroke are presented in figures 4 and 5. The responses of both control valves at ±5-percent stroke indicate a usable control range out to approximately 35 cycles per second. The ±5-percent-stroke curves represent error voltages of approximately ±10 percent of full-scale values and are therefore suitable for use in the analysis of loop stability.

The constants K_1 and K_{11} defining valve travel for a given applied voltage were evaluated by measuring the total travel of each valve with a dial indicator and dividing the travel by the position voltage corresponding to the total travel.

The constants K_2 and K_{12} define the volume flow through each valve for a given valve lift. The values of these constants depend upon the pressure drop across the valves and in general will be different for each run condition. The volume flow rate through the valve was determined from the measurement of the weight-flow rate at each run condition. The corresponding value of the lift was determined from the known area-lift constant and the weight flow and pressure drop across each valve.

Flow pickup, connecting lines, and Venturi. - The natural frequencies of the ΔP pickups and lines were calculated approximately by considering each measuring system as a simple second-order system consisting of an estimated liquid column compressing a trapped volume of gas. From the nature of the solution it was obvious that, in order to make the frequency response of the ΔP pickups as high as possible, the liquid-column length in the lines and the total line length should be made as short as possible. The oxidant ΔP lines, which were 1.5 feet long, were isolated from the liquid-nitrogen bath and electrically heated down close to the Venturi. The fuel pickup lines were considerably longer, approximately 7 feet in length, because the Venturi was located at the end of the dip tube near the bottom of the tank. The calculated natural frequency of the fuel ΔP measuring system was approximately 13 cycles per second, and that of the oxidant system approximately 16 cycles per second.

In order to understand and express the dynamics of the ΔP measuring systems better, an analysis was made of the response, as indicated on an oscillograph recorder, of the fuel and oxidant ΔP pickups to the cutoff step change of each flow at the end of an actual run. This analysis was made in a manner suggested by Chestnut and Mayer (ref. 1) for obtaining the frequency response of a dynamic element when its transient response to a step input is known. In figures 6 and 7 the frequency responses of the fuel and oxidant ΔP measuring systems as obtained from this analysis are presented, and theoretical second-order curves are fitted to these data. The theoretical curve for a damped natural frequency of 15.5 cycles per second and a damping ratio of 0.3 agreed most closely with the analytical results for the fuel ΔP measuring system, and the theoretical curves for

a damped natural frequency of 20 cycles per second and a damping ratio of 0.17 best agreed with the analytical results for the oxidant ΔP system.

There is less correlation between the analytical results for the oxidant ΔP measuring system and the theoretical second-order curve chosen (fig. 7) than for the fuel ΔP measuring system (fig. 6), but this is primarily due to the presence of some extraneous frequencies in the oxidant ΔP trace that made the method of analysis subject to reduced accuracy. The theoretical second-order curves represent the response of the flow-measuring systems adequately for the purpose of this analysis and therefore are used in the subsequent section on loop dynamics.

The steady-state constants K_4 and K_{14} are dependent entirely on the sensitivity of the ΔP pickup and the amplifier gain used for any particular run condition.

The constants K_3 and K_{13} are dependent upon the pressure drop against flow characteristics of the Venturis used and the flow levels. They are computed by taking the slope of the curve of pressure drop against volume flow at the volume-flow point corresponding to each O/F run condition.

Dead time between measuring station and valve. - The dead time in the line is the time for a pressure wave originating at the valve to travel upstream at the velocity of sound of the liquid and appear at the Venturi. For the hydrogen system the line distance between valve and Venturi was approximately 25 feet, and the velocity of sound in liquid hydrogen is approximately 4040 feet per second. The dead time for the hydrogen line is 0.0062 second, obtained by dividing the line length by the velocity of sound in the medium. The reciprocal of the dead time is the frequency at which the phase shift is 360°. Figure 8 is a plot of the relation between phase lag and frequency for a dead time of 0.0062 second. The phase lags due to dead times in the lines between the engine and the hydrogen control valve, the engine and the fluorine control valve, and the fluorine control valve and Venturi were neglected because of the short distances involved.

Engine dynamics. - The dynamic response of the combustion-chamber pressure to changes in propellant flow as a function of frequency was analyzed by the method presented in reference 2. For this engine and propellant combination the dynamic response is flat beyond 100 cycles per second, the upper frequency of interest in the control system. Therefore, the response of chamber pressure to propellant flows is considered to be adequately represented by the constants K_5 and K_{15}, which are the partial of chamber pressure with respect to oxidant flow and the partial of chamber pressure with respect to fuel flow, respectively. The equations for the constants K_5 and K_{15} as a function of engine variables, which are developed in appendix C, are as follows:

$$K_5 = \left.\frac{\partial P_c}{\partial Q_o}\right|_{w_f} = \frac{\rho_o}{A_{th} g}\left[\frac{w_{t,1}}{\Delta w_o}\left(c_2^* - c_1^*\right) + c_2^*\right] \qquad (C10)$$

$$K_{15} = \left.\frac{\partial P_c}{\partial Q_f}\right|_{w_o} = \frac{\rho_f}{A_{th} g}\left[\frac{w_{t,1}}{\Delta w_f}\left(c_2^* - c_1^*\right) + c_2^*\right] \qquad (C9)$$

The constant K_6 is determined by the sensitivity of the chamber-pressure pickup and the gain of the amplifying system. The chamber-pressure pickup was a high-dynamic-response type. It was installed with a short line so that the dynamic response of the pickup was flat to over 200 cycles per second. The dynamics of this system are therefore neglected in this report.

Oxidant-fuel-ratio network. - The constants K_o and K_f are determined from the geometry of the electrical network associated with the O/F potentiometer. This network has no dynamic elements, and therefore its characteristics can be represented by constants. The values of these constants depend upon the setting of the O/F potentiometer.

Loop Dynamics

In order to determine the over-all system stability, it is necessary to examine the open-loop transfer functions for the fuel control loop, the oxidant control loop, and the chamber-pressure control loop. The following detailed analysis is for O/F of 6.14 and P_c of 300 pounds per square inch absolute. The methods used in the analysis are applicable to other O/F conditions.

Fuel control loop. - The rocket engine is started with a fuel-flow lead that must be controlled by the fuel control loop before the system is switched over to chamber-pressure control; therefore, the fuel-control-loop stability is examined first. The fuel control open-loop transfer function of volts out of the ΔP pickup to volts in at the servoamplifier (fig. 3(b)) is obtained by multiplying the amplitude ratios and appropriate constants of each of the elements between the two points and adding their respective phase shifts. Dead time in the line between valve and Venturi will cause a phase lag with no change in amplitude. The amplitude ratio for this transfer function and the associated phase lag are shown in figure 9.

It is clear from figure 9 that the fuel control loop will be unstable if the loop is closed with a proportional gain greater than approximately 0.3, because the amplitude ratio will be greater than unity in the frequency region where the phase lag is equal to or greater than 180°.

However, the expression for the percentage error of a control system

$$\frac{\text{Error}}{\text{Input}} = \frac{1}{1 + G}$$

indicates that the loop gain G_1 must be made 10 or greater before a reasonably small percentage error is obtained. With the requirement that the loop gain be small (approx. 0.3) in the frequencies near resonance, and large (10 or more) in the lower-frequency region corresponding to steady-state operation, an integrator-type control function is indicated. An integrator plots as a 0.1-amplitude-ratio-per-decade line on an amplitude-against-frequency log-log diagram and therefore would provide the necessary high gain at low frequencies and low gain at high frequencies. The control function used was actually proportional-plus-integral, because, by using the servomotor in an unusual way to provide integral control, the presence of a small generator impedance (resistive) in the feedback path resulted in a proportional-plus-integral control rather than a pure integral control. The method of using the servomotor to provide the necessary control function is developed in appendix B.

Figure 10 indicates the amplitude-ratio and phase-lag characteristics of the control function. Figure 11 presents the open-loop transfer function of the fuel control loop with proportional-plus-integral control. With the added control function G_{10}, the resultant open-loop amplitude-ratio response is well below unity in the frequency region where the phase lag passes through 180°.

Oxidant control loop. - It is necessary to examine the oxidant flow-control loop to determine whether the loop by itself is stable when closed before either fuel and O/F control or P_c and O/F control can be achieved. The open-loop transfer function of the oxidant-flow control loop is obtained in the same manner as used in the fuel control-loop analysis (see fig. 3(b)). The amplitude ratios and constants of the elements between the voltage signal into the servoamplifier and the voltage out of the O/F network K_O are multiplied and their phase shifts are added. Figure 12 presents the function and indicates that the loop will be unstable with a proportional gain greater than approximately 0.6. As in the case of the fuel control loop, a proportional-plus-integral control function G_O was added to provide stability when the loop was closed. The characteristics of this control are shown in figure 13. Figure 14, which presents the amplitude-ratio and phase-lag characteristics of the resultant open-loop transfer function with proportional-plus-integral control, indicates that the loop will be stable when closed.

Chamber-pressure control. - Analysis of the chamber-pressure control system is more complex than that of the fuel or oxidant control loops. The open-loop transfer function that must be examined (fig. 3(b)) is the voltage out of the P_c pickup K_6 for a voltage into the fuel controller G_{10}. Because the voltage out of K_6 is proportional to chamber pressure, its value is determined by both the fuel and oxidant propellant flows that are fed into the engine. Therefore, in investigating the P_c open-loop transfer function, two major control loops must be analyzed and their transfer functions must be obtained.

Figure 15 is a simplified block diagram of figure 3(b) indicating these two control loops. One control loop is composed of the forward elements in the fuel control loop ($G_{10}K_{11}G_{11}K_{12}$) and K_{15} and K_6, and its transfer function is the voltage output of K_6 caused by fuel flow to the engine for an input to G_{10}. The other control loop is composed of the fuel-loop forward elements ($G_{10}K_{11}G_{11}K_{12}$), the fuel-loop feedback elements ($K_{13}K_{14}G_{14}e^{-\alpha s}$), the closed-loop oxidant system transfer function (Q_o/v_f), and the constants K_5 and K_6. This transfer function is the voltage out of K_6 caused by oxidant flow for an input to G_{10}.

These two transfer functions are developed in appendix D, and the results are presented in figure 16 together with their vector sum (V_t), which is the over-all transfer function of voltage out of K_6 caused by both propellant flows for an input to G_{10}. The V_t curve indicates that the chamber-pressure control system has a large stability margin if the loop is closed. At the lower frequencies the oxidant control system is the principal contributor to the chamber-pressure system dynamics, while at the higher frequencies the dynamics of the fuel control system predominate.

RESULTS AND DISCUSSION

System Performance

Figure 17 presents a time history of the run for which the control analysis was made. The run consisted of a 2-second fuel-flow lead and four successive O/F points at constant P_c. At the end of the fuel-flow lead, the oxidant-flow control loop was activated and the fuel control loop was switched over to chamber-pressure control, resulting in the first O/F point. Each subsequent O/F was obtained by switching in, by means of a time-delay relay, a separate potentiometer set to the desired value.

Figure 17 indicates that the control system held the steady-state chamber pressure and the steady-state oxidant-fuel ratio to within approximately ±2 percent of the set values. For each step change in O/F, the overshoot was approximately 15 percent of the step, and the time taken to reach the new steady-state set point was approximately 1.5 seconds. These values were considered to achieve the objectives of the research program satisfactorily.

A step change in O/F causes a deviation of chamber pressure from its control point. This deviation is caused by the momentary increase in oxidant flow that occurs when the oxidant-fuel-ratio potentiometer is switched to one set for a higher value. The chamber-pressure control loop then reduces the fuel flow and returns the chamber pressure to its set value at a rate determined by the dynamics of the control loop (fig. 16). The amount of deviation of chamber pressure from its control point was approximately 10 percent, and the time taken to return to the control point was approximately 1.5 seconds. This deviation did not interfere with the objectives of the research program.

Figure 18 presents a time history of a run in which the oxidant-fuel ratio was held constant and the chamber pressure was varied in four successive steps (140, 100, 80, and 60 lb/sq in. abs at engine throat). Each chamber pressure was obtained by switching in, by means of a time-delay relay, a separate potentiometer set for the desired value. For this mode of operation the control system held the steady-state O/F to within ±2 percent of the set value and the steady-state P_c to within approximately ±3 percent of the set values. The response of chamber pressure to a step change in set values is overdamped; therefore, there is no overshoot, and the time taken to reach 63 percent of the difference in set values is approximately 0.3 second. The excessive error in steady-state chamber pressure can be attributed to the fact that in this run an instrumentation limitation made it necessary to use a full-scale chamber-pressure value of 400 pounds per square inch gage, which caused any control or instrumentation-system zeroing errors to appear as an appreciable error in chamber-pressure control. The errors in steady-state chamber pressures shown are actually less than 1 percent of full-scale value of chamber pressure.

It is also to be noted in figure 18 that, during a step from one set value of P_c to a lower one, there is a momentary increase in O/F. The reason for this increase is that the action of the chamber-pressure control loop is to reduce the fuel flow and that the oxidant flow must follow the reduction in fuel flow at a rate determined by the dynamics of the O/F control system. The deviation in O/F from the set point during each stepping of P_c was approximately 12 percent, and the time taken to return to the set value was approximately 2 seconds.

Figures 17 and 18 indicate that the response of the chamber-pressure control loop is very much overdamped. This situation could have been predicted from figure 16, which indicates that the speed of response of the chamber-pressure control loop could be increased several times without instability. Therefore, for later runs the integration rate of the fuel controller G_{10} was modified so that, upon switchover from fuel-lead flow control to chamber-pressure control, its value was increased three times. Figure 19 is a time history of a run incorporating this modification in which P_c was held constant and O/F was varied in two steps. The steady-state chamber pressure was held to within ± 0.5 percent of the set value, and the steady-state oxidant-fuel ratios were held to within ± 1.5 percent of the set values. The deviation of chamber pressure from its set value during O/F switchover is approximately the same as indicated in figure 17, but the time taken to return to the set value has been reduced to 0.5 second, as compared to 1.5 seconds in figure 17. No variable-chamber-pressure run has been made with this configuration, but theoretically the response of chamber pressure to a step change in set values should be three times as fast.

Starting and Switchover Transients

Figure 20 is a time history to an expanded scale of the startup of the variable-chamber-pressure run shown in figure 18. The low level of propellant flows led to the worst startup condition encountered in the test program, and for this reason the startup for this run is presented. As seen in figure 20, there is a considerable delay in the rise of chamber pressure after the oxidant-flow system is activated and the control system switched over from fuel control to chamber-pressure control. The reason for this delayed rise in chamber pressure is that, after the oxidant control valve is opened, the oxidant flow must first fill the volume between the control valve and injector face before being injected into the engine. The rate at which the volume is filled is determined by the instantaneous oxidant-flow rate. Therefore, for runs at low chamber pressures, in which the corresponding oxidant flow is low, the time taken to fill the volume is increased. The result of the delayed rise in chamber pressure is a situation in which the control system cannot adequately control chamber pressure and oxidant-fuel ratio. Consideration of the actions of the P_c and O/F control loops makes the reason for the lack of adequate control apparent.

When the system is switched over from fuel-lead flow control to chamber-pressure control and the oxidant-flow system is activated, the initial value of chamber pressure is essentially atmospheric; therefore, a large error exists between actual and desired chamber pressure. This error voltage causes the fuel control valve to open rapidly - in the case shown in figure 20 to its full-open position - making the O/F

control open the oxidant control valve rapidly in an effort to obtain the desired oxidant-fuel ratio. The rapid rise in oxidant flow causes the resultant O/F to overshoot the set value, and oscillation in O/F results. The situation would not be as unfavorable if chamber pressure rose rapidly upon switchover; but, because of the delayed rise in chamber pressure, the propellant flows, in addition to being oscillatory about a set O/F, are far over the amount necessary to obtain the desired chamber pressure. An overshoot in chamber pressure results. The chamber-pressure control loop must then reduce fuel flow and consequently oxidant flow until the chamber pressure is equal to the set value. As pointed out before, this run exhibited the worst startup transients because the initial levels of propellant flow were low. In other runs, such as the one presented in figure 17, in which the desired chamber pressure was higher, the transients encountered in startup were less severe but nonetheless present.

The transients encountered in startups can be alleviated by delaying the switchover from fuel-lead flow control to chamber-pressure control until the chamber pressure has risen to approximately the set value. With this mode of operation, the value of the fuel-flow lead was selected to correspond to the amount that would produce, with the oxidant flow in the proper O/F, the desired chamber pressure. Figure 21 shows the first second of the run presented in figure 19 to an expanded time scale, in which the switchover to chamber pressure was delayed 0.5 second after the oxidant controller was energized. The resulting start is much smoother and results in no undesirable oscillation in either chamber pressure or oxidant-fuel ratio.

CONCLUDING REMARKS

This report describes a control system that is capable of starting a hydrogen-fluorine rocket engine, of providing stable operation to within ±2 percent of the preset values of chamber pressure and oxidant-fuel ratio (O/F), and of limiting transient deviations in O/F sufficiently to avoid a stoichiometric mixture. In addition, the control system is capable of multipoint stepping of oxidant-fuel ratio and chamber pressure through any range within the rocket-engine and instrumentation-system capability. The speed of response of the control-valve actuators used was more than adequate to meet emergency shutdown safety requirements.

The control system performed accurately and rapidly enough to provide good engine data. However, the speed of response was limited by the frequency at which an underdamped second- or higher-order resonance occurred in each control loop. The existence of this resonance necessitated the use of integral control with as small a proportional component as possible (considerably less than 1). The primary source of the resonance was the flow-measuring system, composed of a Venturi, ΔP pickup, and connecting lines. The underdamped response of the flow-measuring

system is caused by the inductance of the slug of liquid and the capacitance of the trapped volume of gas in the ΔP pickup and connecting lines. This resonance problem will be encountered in cryogenic systems unless means are employed to keep the ΔP pickup and connecting lines either completely full of liquid or completely full of gas.

Lewis Research Center
National Aeronautics and Space Administration
Cleveland, Ohio, July 17, 1959

APPENDIX A

SYMBOLS

A_{th} area of engine nozzle throat, sq in.

c^* characteristic exhaust velocity, ft/sec

G_l frequency-dependent transfer function of an entire control loop

G_O frequency-dependent transfer function of oxidant controller

G_{lO} frequency-dependent transfer function of fuel controller

G_1 frequency-dependent transfer function of oxidant servovalve

G_{11} frequency-dependent transfer function of fuel servovalve

G_4 frequency-dependent transfer function of oxidant ΔP pickup and lines

G_{14} frequency-dependent transfer function of fuel ΔP pickup and lines

g acceleration due to gravity, 32.178 ft/sec^2

K_f steady-state gain of O/F output to fuel signal input, v/v

K_o steady-state gain of O/F output to oxidant signal input, v/v

K_1 steady-state gain of oxidant servomotor, in./v

K_{11} steady-state gain of fuel servomotor, in./v

K_2 steady-state gain of oxidant valve, (cu in./sec)/in.

K_{12} steady-state gain of fuel valve, (cu in./sec)/in.

K_3 steady-state gain of oxidant Venturi, (lb/sq in.)/(cu in./sec)

K_{13} steady-state gain of fuel Venturi, (lb/sq in.)/(cu in./sec)

K_4 steady-state gain of oxidant ΔP pickup, v/(lb/sq in.)

K_{14} steady-state gain of fuel ΔP pickup, v/(lb/sq in.)

K_5 steady-state value of partial of chamber pressure with respect to oxidant volume flow, (lb/sq in.)/(cu in./sec)

K_{15} steady-state value of partial of chamber pressure with respect to fuel volume flow, (lb/sq in.)/(cu in./sec)

K_6 steady-state gain of chamber-pressure pickup, v/(lb/sq in.)

O/F ratio of oxidant flow to fuel flow by weight

ΔP flow-measuring Venturi pressure drop, lb/sq in.

P_c total pressure in combustion chamber measured at throat, lb/sq in. abs

Q volume flow, cu in./sec

s dimensionless complex operator

t time, sec

V_f open-loop transfer function of voltage out of K_6 caused by fuel flow for an input to G_{10}

V_o open-loop transfer function of voltage out of K_6 caused by oxidant flow for an input to G_{10}

V_t open-loop transfer function of chamber-pressure control loop

v_f voltage out of fuel ΔP pickup, v

w weight flow, lb/sec

α dead time, sec

ρ density, lb/cu in.

Subscripts:

f fuel

o oxidant

t total

1,2 different operating conditions

APPENDIX B

DESCRIPTION OF COMPONENTS AND OPERATION

The construction details of the electrohydraulic actuator and the electronic servoamplifier circuitry are discussed herein. Details of some of the techniques used in the control system are also presented.

Servo-Operated Control Valve

Actuator and valve assembly. - The electrohydraulic actuators for the propellant control valves were identical. The actuator consists of a piston assembly, a Moog Electrohydraulic Servovalve, and a Schaevitz Linear Variable Differential Transformer for position pickup. Figure 22 presents a disassembled view and figure 23 an exploded view of the actuator components. All housings, end plates, and the mounting yoke are made of aluminum. The piston and shaft are made of stainless steel. No special bearings are used. The stainless-steel piston and shaft running in aluminum housings and end plates form satisfactory bearing surfaces. Both static and dynamic seals are formed by O-rings. Where high pressures are involved, Teflon backup rings are used.

In figure 22 a small piston with O-rings is shown on the right end of the piston shaft. The cylinder for this piston is formed in the left end of the mounting yoke. This piston and cylinder assembly is pressurized by gas to hold the control valve closed during the long periods of preparation of the propellant system prior to firing. This separate valve-closing system makes it unnecessary to operate the electrohydraulic servo system during these periods with the attendant chance of failure of electronic or hydraulic components. This piston is not pressurized when the automatic control system is in operation.

The small transformer shown in figure 22 is used to transform the relatively high impedance of the position pickup down to a low value suitable for transmission over long distances without phase shift of the signal.

The actuator is shown in its assembled form in figure 24 and in mock-up form mounted on the control valve in figure 25. The actuator is fastened to the valve by screwing the valve shaft into the hexagonal nut on the end of the piston shaft and clamping the mounting yoke to the valve body by means of the wedging collar shown in figures 22 and 23. The method of attachment is more apparent from figure 26, which shows the actual fluorine control valve used in the test program. Because this actuator was not available for disassembly, a redesigned unit is presented in figures 22 to 25. The redesigned actuator is similar in construction and

identical in dynamic performance. The redesign involved only machining and space economies.

The control valve for each propellant consists of a standard plug-type valve body equipped with a linear plug and seat assembly and appropriate seals. The fluorine valve shown in figure 26 is a standard 1.5-inch valve and incorporates a bellows shaft seal. The hydrogen valve, not visible at the left in figure 26 behind its shield, uses a Teflon packing shaft seal. It also was a standard 1.5-inch valve but was changed in later tests to a 0.75-inch valve.

The stroke of the actuator and valve assembly used in the test program is 0.5 inch. For conditions in which the standard valve plug required a stroke above 0.5 inch to obtain full-open area, the plug was altered so that full-open area was obtained in 0.5 inch. It is desirable to use short strokes in servomotors of this kind, because reasonable percentages of full stroke are then attainable with good linearity and high frequency response. The excellent positioning ability of this type of servomotor makes it feasible to design for short strokes.

The hydraulic pressure was supplied to both units at 1500 pounds per square inch by an electric-driven vane-type pump with a relief valve and accumulator. 10-Micron filters were used ahead of each valve actuator.

The area of the piston was approximately 1 square inch. The piston was equipped with an O-ring to minimize leakage across it. The full-scale flow from the Moog Servovalve was approximately 28 cubic inches per second.

Electronic servoamplifier. - A schematic diagram of the electronic servoamplifier is shown in figure 27. The position pickup is energized from the carrier oscillator and produces an a-c voltage proportional to the displacement from center with a polarity that is either in phase or out of phase with the oscillator, depending upon direction from center. The stepdown and step-up transformer system enables the position signal to be transmitted at low impedance over the long lines without appreciable phase shift. The position signal from the output of the step-up transformer is added to the signal from the manual-position potentiometer, and the resulting error signal is demodulated to obtain a d-c voltage proportional to position error. The error signal is introduced to the d-c amplifier, which produces a differential torque-motor current that in turn produces a hydraulic flow to one side of the actuator piston, causing a piston velocity.

The steady-state characteristics of this loop are such that there will be a valve position for every setting of the manual-position potentiometer. The valve may also be positioned by introducing a d-c voltage at the servoamplifier input. There will be a unique relation of input voltage against valve position for each manual-position setting. In the control system

described in this report, the manual-position potentiometer was set so that with zero voltage at the input the valve was held closed. This satisfied the safety requirement that the valve should return to a closed position upon programmed or emergency system cutoff. The frequency response of valve position to input voltage is presented in figures 4 and 5.

Control-System Details

Figure 28 is a schematic diagram of the complete system. This diagram shows the method of obtaining integral control, the method of setting O/F, the fuel-lead and chamber-pressure control points, and the relays used to activate the system.

The method of obtaining integral control was unusual because, instead of using a conventional electronic integrator employing an operational amplifier, capacitor feedback, and resistor input, the integral control shown here makes use of the gain of the servomotor loop. Thus, by inserting a capacitor in place of resistor R_f shown in figure 27, the servomotor loop becomes a system that integrates the voltage at the input; that is, it produces a valve velocity proportional to the input voltage. By making the input voltage the control error voltage, the servomotor will integrate the error toward zero at a rate determined by the values of resistor R_i and capacitor C_f. In the actual circuit, the generator impedance of the demodulator producing the valve position voltage appears as a small resistance in series with the feedback capacitor, making the control action proportional-plus-integral instead of pure integral. As shown in figures 10 and 13, the proportional gain is small (considerably less than 1) but has been further reduced in a later design to provide an increased stability margin for this type of resonant control loop.

The control error voltage is obtained in the case of the fuel-lead and chamber-pressure control system by the use of a standard bucking circuit in series with the control signals, as shown in figure 28. The bucking circuit is formed by a battery and adjusting resistor to provide the negative of the full-scale control-signal voltage across the ten-turn set-point potentiometer. The action of the circuit is such that the voltage at the wiper arm of the set-point potentiometer is equal to the difference between the existing percentage of full-scale control-signal voltage and the desired percentage set on the potentiometer.

The voltage usable as an O/F error signal is obtained by feeding the fuel and oxidant ΔP signals to opposite ends of the ten-turn O/F potentiometer. By making the oxidant ΔP voltage the negative of the fuel ΔP voltage, the voltage at the wiper arm of the potentiometer becomes the difference between the percentage of full-scale values of the fuel and oxidant ΔP signals. The desired O/F set on the potentiometer

is obtained when the fuel and oxidant ΔP voltages are in the ratio of the resistances between the wiper arm and the corresponding ends of the potentiometer. For this condition the voltage appearing at the wiper arm is zero and there is no control error.

While the system is not in automatic control, the valve servomotors are locked to a closed position by means of the relays shown, which ground the inputs and short the feedback capacitors. The control system is activated by energizing relay r_1, which provides voltage to the fuel and chamber-pressure set-point potentiometers and unlocks the fuel-valve servomotor, allowing it to respond to the fuel error signal. Following the prescribed period of fuel-lead precool, relay r_2 is energized to unlock the oxidant-valve servomotor, allowing it to respond to the O/F error signal. Relay r_2 also shifts control from fuel-flow control to chamber-pressure control. At the end of the run program or upon emergency shutdown, relays r_1 and r_2 are deenergized and the valves return to closed position in a maximum of 20 milliseconds. The relays are sequentially timed by a control timer in the rocket test-cell control room.

The accuracy of the control system is determined by the accuracy and linearity of the instrumentation providing the control signals, the accuracy with which the full-scale setting potentiometer voltages can be matched to the full-scale control-signal voltages, the linearity of the setting potentiometers, and the drift characteristics of the d-c amplifiers and servovalves. Shortly before the run, each d-c amplifier is balanced so that zero piston velocity is obtained for zero input to the amplifier corresponding to zero error. Any drift in the amplifier or servovalve system that would require a voltage other than zero at the input of the d-c amplifier to obtain zero piston velocity would cause the control system to hold a point different from that set on the potentiometer. The drift characteristics of the d-c amplifiers employed were sufficiently low that this error was less than 0.5 percent. Even with reasonably low drift characteristics, it is desirable to balance the d-c amplifiers as close to run time as possible. However, it is not feasible to allow the propellant valves to drift open at this stage of run preparation. Therefore, a system of resistors duplicating the torque-motor coil resistances was inserted in the plate circuit as shown in figure 28. The values of these resistors had been previously chosen to obtain a zero galvanometer deflection at the same condition of d-c amplifier balance, which resulted in zero piston velocity when the amplifier was connected to the torque-motor coils. This resistor network and the galvanometer are used to balance the d-c amplifier before a run without opening the propellant valves.

This circuit also lends itself to providing a safe "standby" position, because all the electronic circuits are disconnected from the torque-motor

coils and a battery is connected across the torque-motor coils to hold the valve in a closed position. Thus, any failure of electronic equipment would not inadvertently open the valves. In addition, the galvanometer indicates the correct operation of the servoamplifier prior to switchover to run condition.

The analysis has indicated that a considerably faster speed of response can be employed in the chamber-pressure control loop than in the fuel control loop. In later runs the chamber-pressure control loop was speeded up by shifting a portion of resistor R_i to a position between the fuel-lead setting potentiometer and the switchover relay r_{2a}. This action left the speed of the fuel control loop the same but increased the response speed of the chamber-pressure control loop.

The RESULTS AND DISCUSSION section has pointed out the desirability of delaying the switchover to chamber-pressure control until the oxidant flow has had sufficient time to fill the line and bring chamber pressure approximately up to the set value. The delay was accomplished by the use of a time-delay relay in place of r_{2a} and activated by r_{2a}.

Multipoint running was obtained by switching in a series of O/F potentiometers and/or a series of P_c potentiometers by means of relays activated by a sequential timer.

APPENDIX C

ENGINE DYNAMICS ANALYSIS

The equations necessary to determine the constants K_5 and K_{15}, which are the partial of chamber pressure with respect to oxidant flow and the partial of chamber pressure with respect to fuel flow, respectively, are developed from the basic equation for characteristic exhaust velocity as a function of engine parameters:

$$c^* = \frac{P_c A_{thg}}{w_t} \tag{C1}$$

Rearranging equation (C1) results in

$$P_c = \frac{c^* w_t}{A_{thg}} \tag{C2}$$

The relation between the chamber pressure at two different operating conditions (i.e., change in O/F) can be expressed as follows:

$$\Delta P_c = P_{c,2} - P_{c,1} \tag{C3}$$

Substituting $P_{c,1}$ and $P_{c,2}$ from equation (C2) in equation (C3) results in

$$\Delta P_c = \frac{c_2^* w_{t,2}}{A_{thg}} - \frac{c_1^* w_{t,1}}{A_{thg}}$$

or

$$\Delta P_c = \frac{1}{A_{thg}} \left[c_2^* w_{t,2} - c_1^* w_{t,1} \right] \tag{C4}$$

However,

$$w_{t,2} = w_{t,1} + \Delta w_t$$

so that

$$\Delta P_c = \frac{1}{A_{thg}} \left[c_2^* (w_{t,1} + \Delta w_t) - c_1^* w_{t,1} \right]$$

or

$$\Delta P_c = \frac{1}{A_{th} g} \left[w_{t,1}(c_2^* - c_1^*) + \Delta w_t c_2^* \right] \tag{C5}$$

Dividing equation (C5) by Δw_t gives

$$\frac{\Delta P_c}{\Delta w_t} = \frac{1}{A_{th} g} \left[\frac{w_{t,1}}{\Delta w_t} (c_2^* - c_1^*) + c_2^* \right] \tag{C6}$$

When the change in total flow is accomplished by variation of fuel flow at constant oxidant flow, equation (C6) can be written as follows:

$$\left. \frac{\partial P_c}{\partial w_f} \right|_{w_o} = \frac{1}{A_{th} g} \left[\frac{w_{t,1}}{\Delta w_f} (c_2^* - c_1^*) + c_2^* \right] \tag{C7}$$

and for variable oxidant flow at constant fuel flow, equation (C6) becomes

$$\left. \frac{\partial P_c}{\partial w_o} \right|_{w_f} = \frac{1}{A_{th} g} \left[\frac{w_{t,1}}{\Delta w_o} (c_2^* - c_1^*) + c_2^* \right] \tag{C8}$$

The constants K_5 and K_{15} are defined as the response of chamber pressure to volume flow of the propellants. Equations (C7) and (C8) may be written for the response of chamber pressure to volume flow by substituting the following relations for w_f and w_o:

$$w_f = Q_f \rho_f$$

$$w_o = Q_o \rho_o$$

With these substitutions, and noting that the resulting partials are equal to K_5 and K_{15}, equations (C7) and (C8) become

$$K_{15} = \left. \frac{\partial P_c}{\partial Q_f} \right|_{w_o} = \frac{\rho_f}{A_{th} g} \left[\frac{w_{t,1}}{\Delta w_f} (c_2^* - c_1^*) + c_2^* \right] \tag{C9}$$

and

$$K_5 = \left. \frac{\partial P_c}{\partial Q_o} \right|_{w_f} = \frac{\rho_o}{A_{th} g} \left[\frac{w_{t,1}}{\Delta w_o} (c_2^* - c_1^*) + c_2^* \right] \tag{C10}$$

The constants K_5 and K_{15} can be evaluated from equations (C9) and (C10) for an assumed change in fuel or oxidant flow by substitution of the values for the several engine and propellant parameters. The combustion-chamber pressure is 300 pounds per square inch absolute, and the area of the engine throat is 12.01 square inches. Density of liquid hydrogen at the control valve is 0.00256 pound per cubic inch, and the density of liquid fluorine is 0.0556 pound per cubic inch. Using data contained in reference 3, a plot was made of theoretical c* as a function of O/F for P_c of 300 pounds per square inch absolute (fig. 29). For O/F of 6.14, corresponding to the first operating condition, the c* value obtained from figure 29 is 8365 feet per second. From equation (C1) the total propellant weight flow is calculated to be 13.84 pounds per second. Of the total weight flow, the fuel weight flow is 1.94 pounds per second, and the oxidant weight flow is 11.9 pounds per second. If an assumed 10-percent decrease in O/F is made, from 6.14 to 5.53, keeping the oxidant flow constant, the increase in fuel flow necessary can be determined by the following equations:

At O/F of 6.14,

$$w_{f,1} = \frac{1}{6.14} w_o \tag{C11}$$

At O/F of 5.53,

$$w_{f,2} = \frac{1}{5.33} w_o \tag{C12}$$

The change in fuel flow from O/F of 6.14 to 5.53 with oxidant flow constant is given by

$$\Delta w_f = w_{f,2} - w_{f,1} \tag{C13}$$

Substituting the values of $w_{f,1}$ and $w_{f,2}$ from equations (C11) and (C12) into equation (C13) gives

$$\Delta w_f = w_o \left(\frac{1}{5.53} - \frac{1}{6.14} \right) = 0.2143 \text{ lb/sec} \tag{C14}$$

where w_o was previously found to be 11.9 pounds per second.

The value of c_1^* at O/F = 6.14 was previously determined from figure 29 to be 8365 feet per second. The characteristic velocity c_2^* is determined by drawing a line tangent to the c* curve at O/F = 6.14 and evaluating c_2^* at the intersection of this line and the line for

O/F = 5.53; c_2^* is found to be 8398 feet per second. The change, then, in c* for the assumed 10-percent change in O/F is 33 feet per second. Equation (C9) can now be evaluated to obtain the constant K_{15} for O/F of 6.14; K_{15} is found to be 0.0698 pound per square inch per cubic inch per second. In a similar manner, the constant K_5 can be evaluated for O/F = 6.14 where fuel flow is held constant and oxidant flow reduced to produce a 10-percent decrease in O/F.

The values of K_5 and K_{15} for O/F = 6.14 are presented in table I. The values of K_5 and K_{15} obtained for changes in P_c resulting from assumed changes in O/F about the other operating points (O/F of 9.0, 11.5, 15.67) are also presented in table I.

APPENDIX D

LOOP DYNAMICS

The transfer function of voltage out of K_6 for an input to the fuel controller G_{10} caused by fuel flow is presented in figure 16. It was obtained by multiplying the transfer function of the forward elements in the fuel control loop ($G_{10}K_{11}G_{11}K_{12}$) as shown in figure 30 by the constants K_{15} and K_6 (see fig. 15).

In the analysis of the portion of the chamber-pressure control loop that is dependent upon oxidant flow (see fig. 15), the amplitude-ratio and phase-lag characteristics of the voltage out of the fuel ΔP pickup to a voltage applied at G_{10} have already been determined (fig. 11). It is now necessary to determine the transfer function of oxidant flow to a fuel ΔP voltage into the O/F network at K_f. As seen in figure 3(b), the oxidant flow is equal to the product of the error voltage and the transfer function of the forward elements in the oxidant loop as follows:

$$Q_o = (\text{Error voltage})G_0K_1G_1K_2 \qquad (D1)$$

The error-voltage input to G_0 is equal to $v_fK_f - Q_oK_3K_4G_4K_o$, where v_f is the voltage out of the fuel ΔP pickup. Substituting for error voltage in equation (D1) and solving for Q_o/v_f gives

$$\frac{Q_o}{v_f} = \frac{K_fK_1G_1K_2G_0}{1 + K_1G_1K_2K_3K_4G_4K_oG_0}$$

as the desired transfer function. This expression was solved by expressing the transfer function of the numerator in terms of its amplitude ratio and phase shift, determining the denominator by adding vertorially 1 to the oxidant open-loop response curves shown in figure 14, and dividing the amplitude ratio of the numerator by the denominator and subtracting their phase shifts. Figure 31 shows the amplitude ratio and phase shift for the transfer function Q_o/v_f. Figure 32 presents the transfer function of oxidant flow to an error-voltage input to the fuel controller G_{10}. This function is obtained by combining the transfer functions shown in figures 11 and 31. By multiplying the transfer functions shown in figure 32 by constants K_5 and K_6, the frequency response of voltage out of K_6 to a voltage input to G_{10} caused by oxidant flow is determined. The results are given in figure 16.

REFERENCES

1. Chestnut, Harold, and Mayer, Robert W.: Servomechanisms and Regulating System Design. Vol. II. John Wiley & Sons, Inc., 1955.

2. Hurrell, Herbert G.: Analysis of Injection-Velocity Effects on Rocket Dynamics and Stability. NASA TR R-43, 1959.

3. Gordon, Sanford, and Huff, Vearl N.: Theoretical Performance of Liquid Hydrogen and Liquid Fluorine as a Rocket Propellant. NACA RM E52L11, 1953.

TABLE I. - CONSTANTS

Constants	Oxidant-fuel ratio, O/F			
	6.14	9.00	11.50	15.67
K_f, v/v	0.447	0.640	0.729	0.822
K_o, v/v	.552	.360	.271	.177
K_1, in./v	.242	.242	.242	.242
K_{11}, in./v	.242	.242	.242	.242
K_2, $\frac{\text{cu in./sec}}{\text{in.}}$	702	680	670.4	636.1
K_{12}, $\frac{\text{cu in./sec}}{\text{in.}}$	3550	4030	4310	4860
$K_3\left(\frac{2\Delta P}{Q}\right)$, $\frac{\text{lb/sq in.}}{\text{cu in./sec}}$	.619	.678	.707	.772
$K_{13}\left(\frac{2\Delta P}{Q}\right)$, $\frac{\text{lb/sq in.}}{\text{cu in./sec}}$	.1108	.0805	.0692	.0589
K_4, $\frac{\text{v}}{\text{lb/sq in.}}$	.00833	.00833	.00833	.00833
K_{14}, $\frac{\text{v}}{\text{lb/sq in.}}$	.01667	.01667	.01667	.01667
K_5, $\frac{\text{lb/sq in.}}{\text{cu in./sec}}$	1.27	1.28	1.25	1.27
K_{15}, $\frac{\text{lb/sq in.}}{\text{cu in./sec}}$	.0698	.0873	.0913	.135
K_6, $\frac{\text{v}}{\text{lb/sq in.}}$	.002	.002	.002	.002

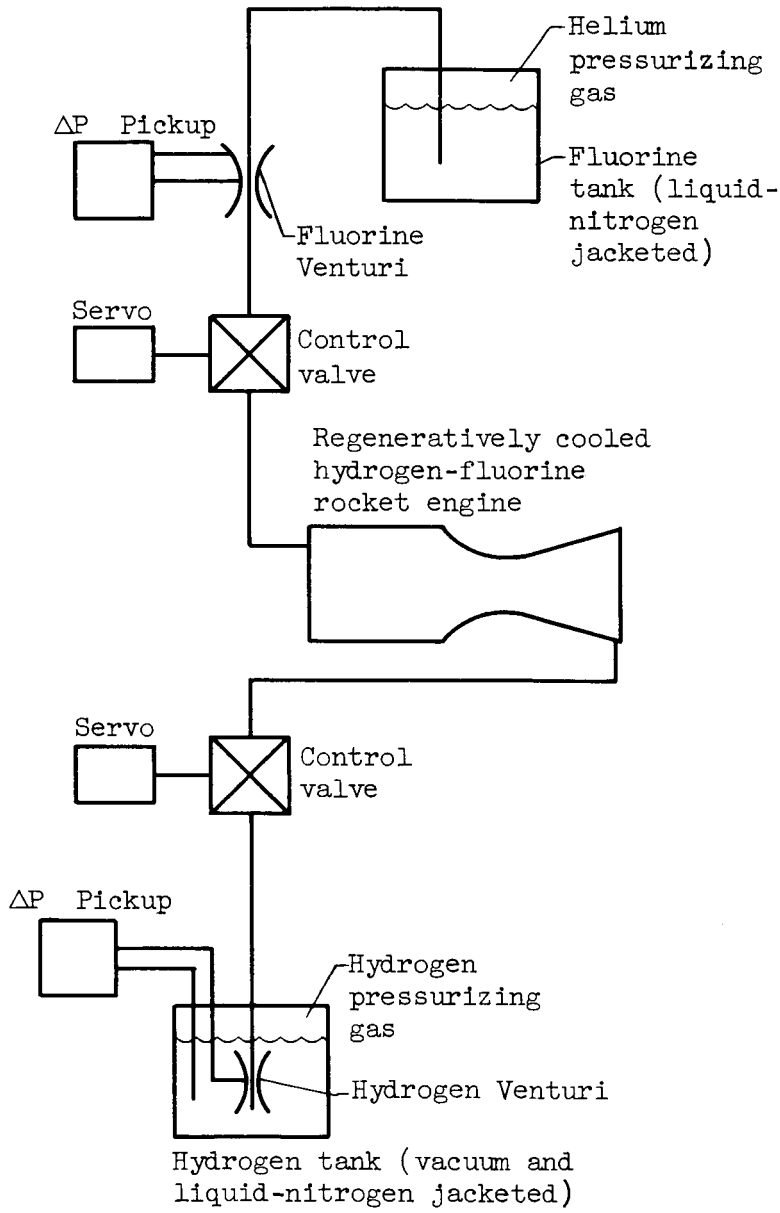

Figure 1. - Schematic diagram of rocket engine and propellant feed system.

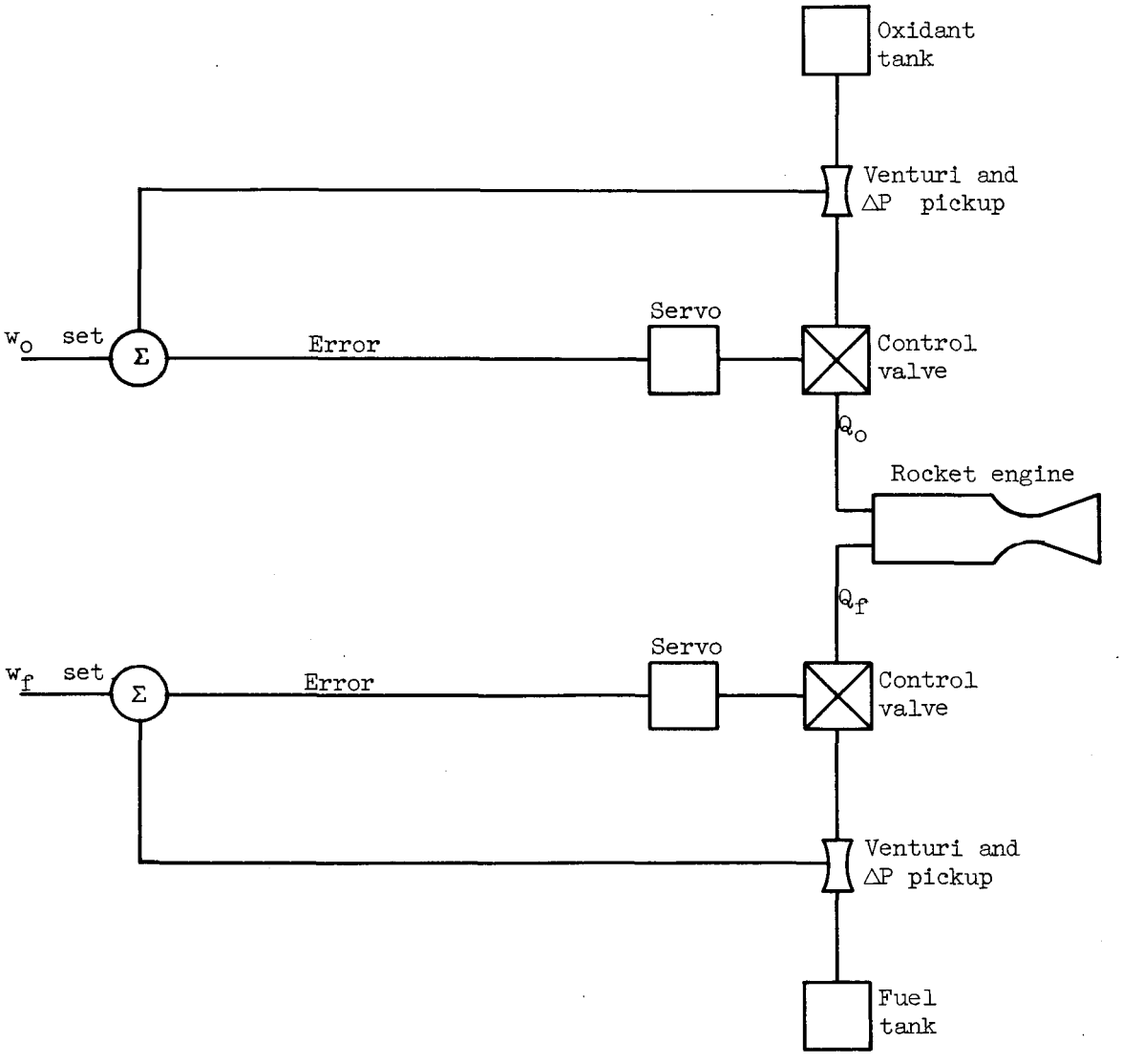

(a) Independent flow control of propellants.

Figure 2. - Schematic diagram of rocket-engine flow-control system.

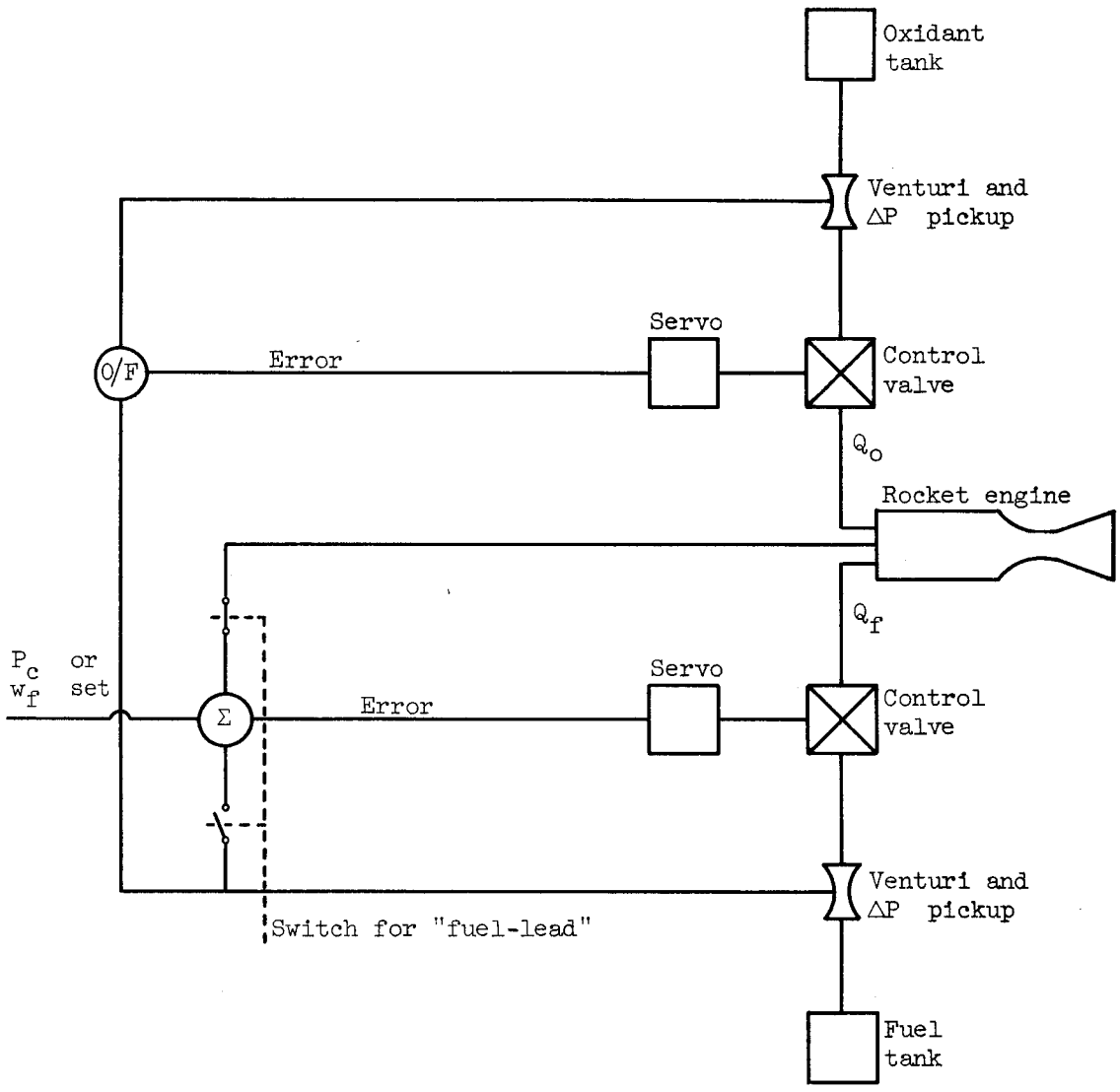

(b) Chamber-pressure and oxidant-fuel-ratio control of propellants.

Figure 2. - Concluded. Schematic diagram of rocket-engine flow-control system.

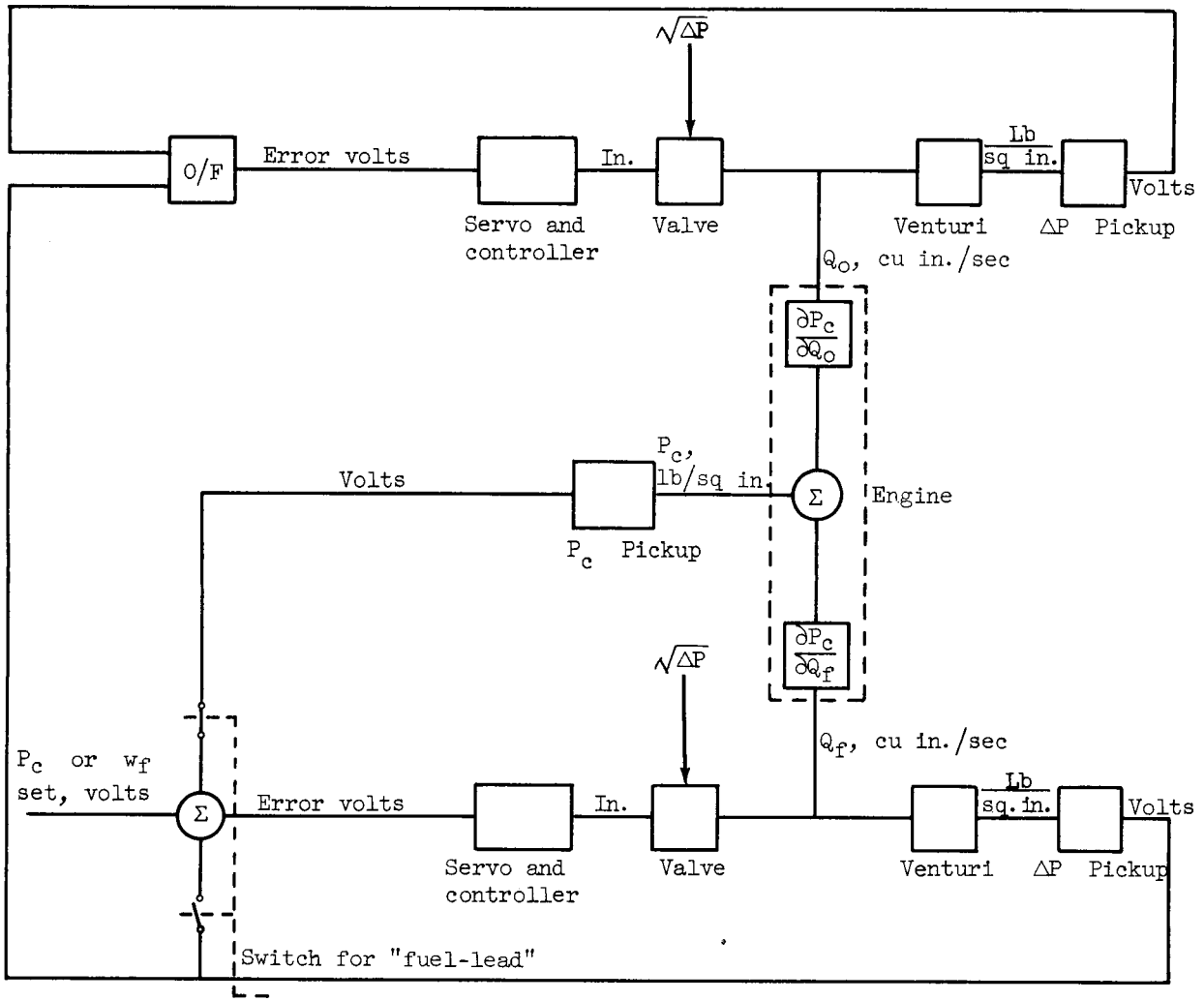

(a) Simplified block diagram.

Figure 3. - Block diagram of system with chamber-pressure and oxidant-fuel-ratio control.

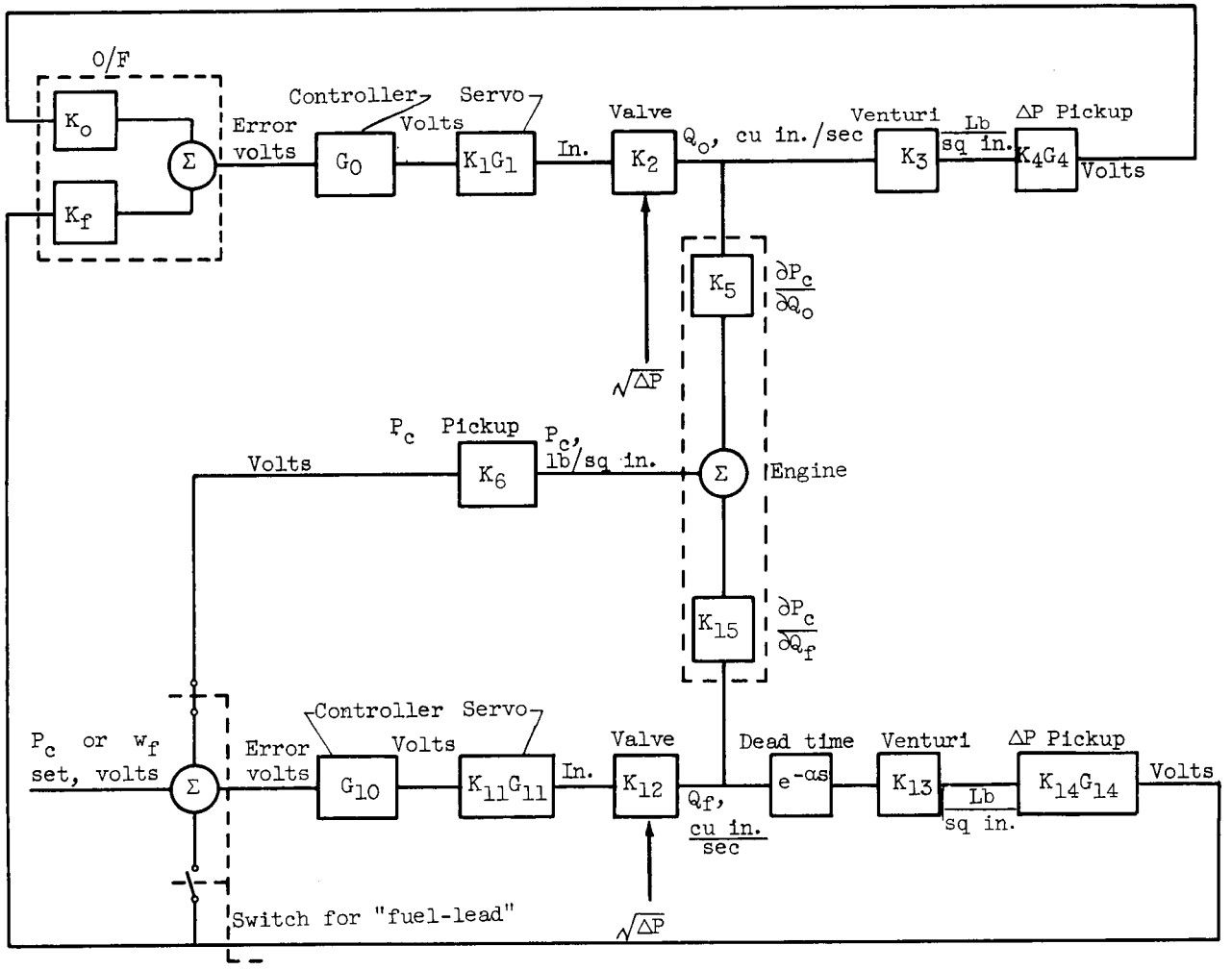

(b) Detailed block diagram indicating approximate form of dynamic response of each component.

Figure 3. - Concluded. Block diagram of system with chamber-pressure and oxidant-fuel-ratio control.

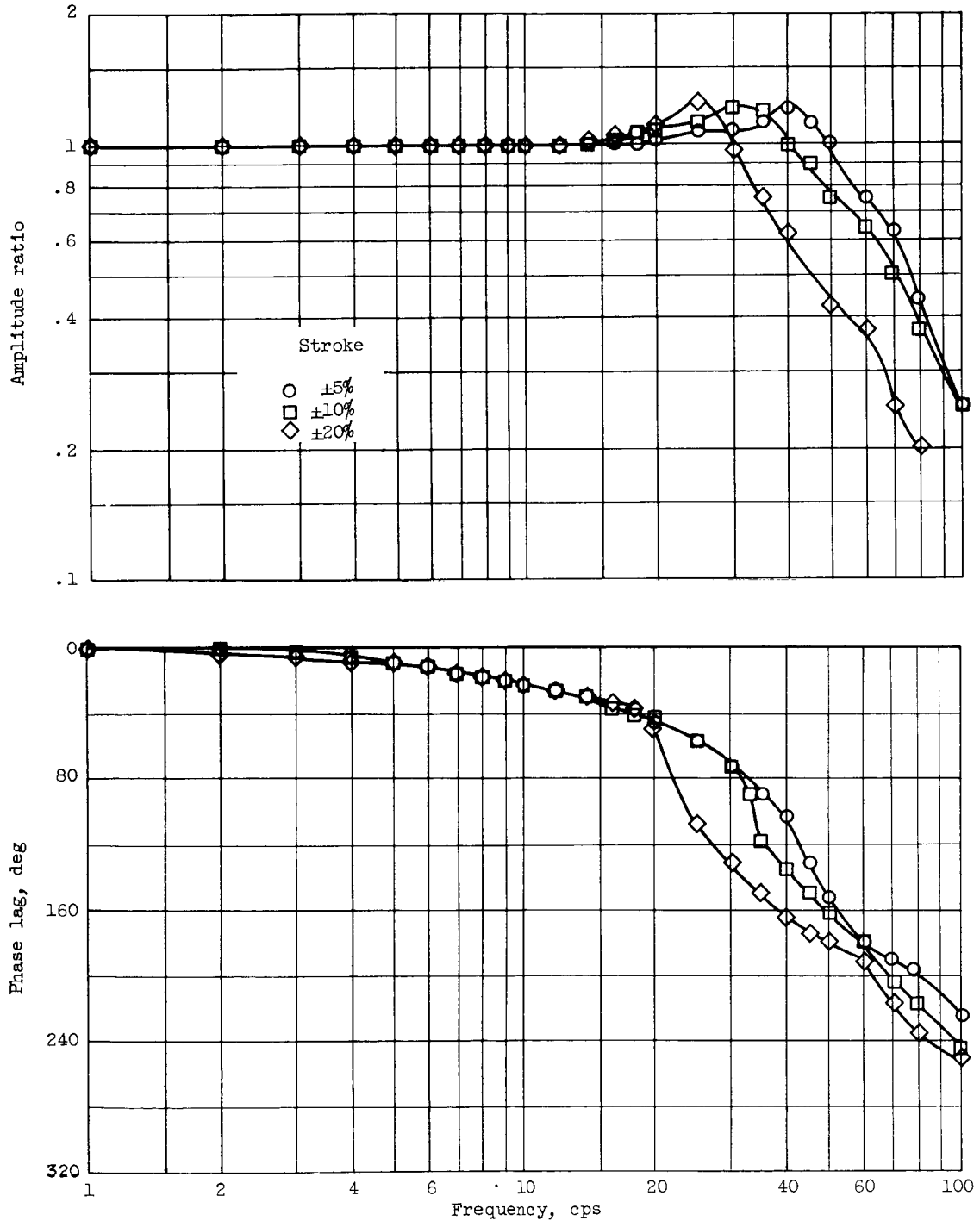

Figure 4. - Frequency response of electrohydraulic servomotor and fuel valve (G_{11}).

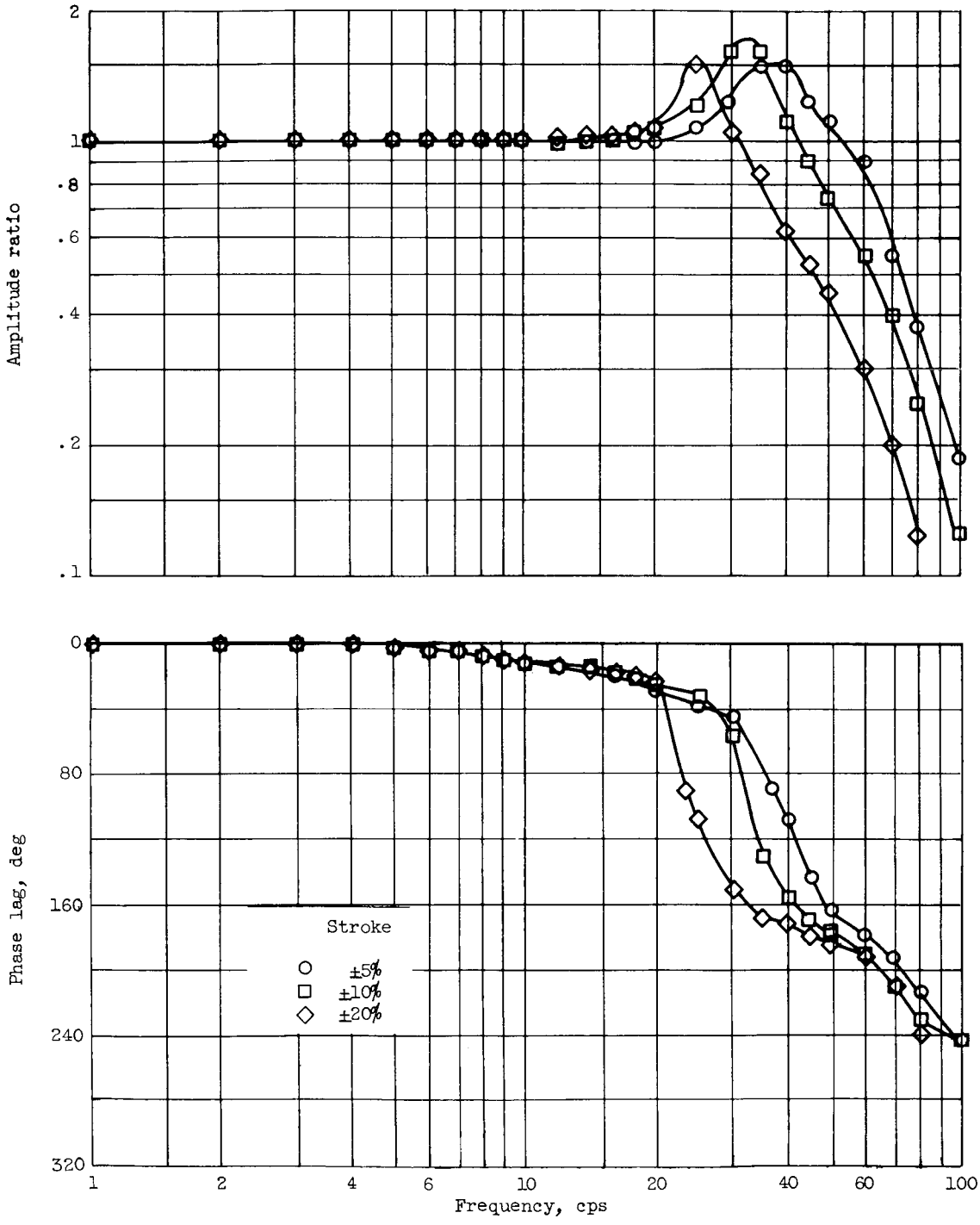

Figure 5. - Frequency response of electrohydraulic servomotor and oxidant valve (G_1).

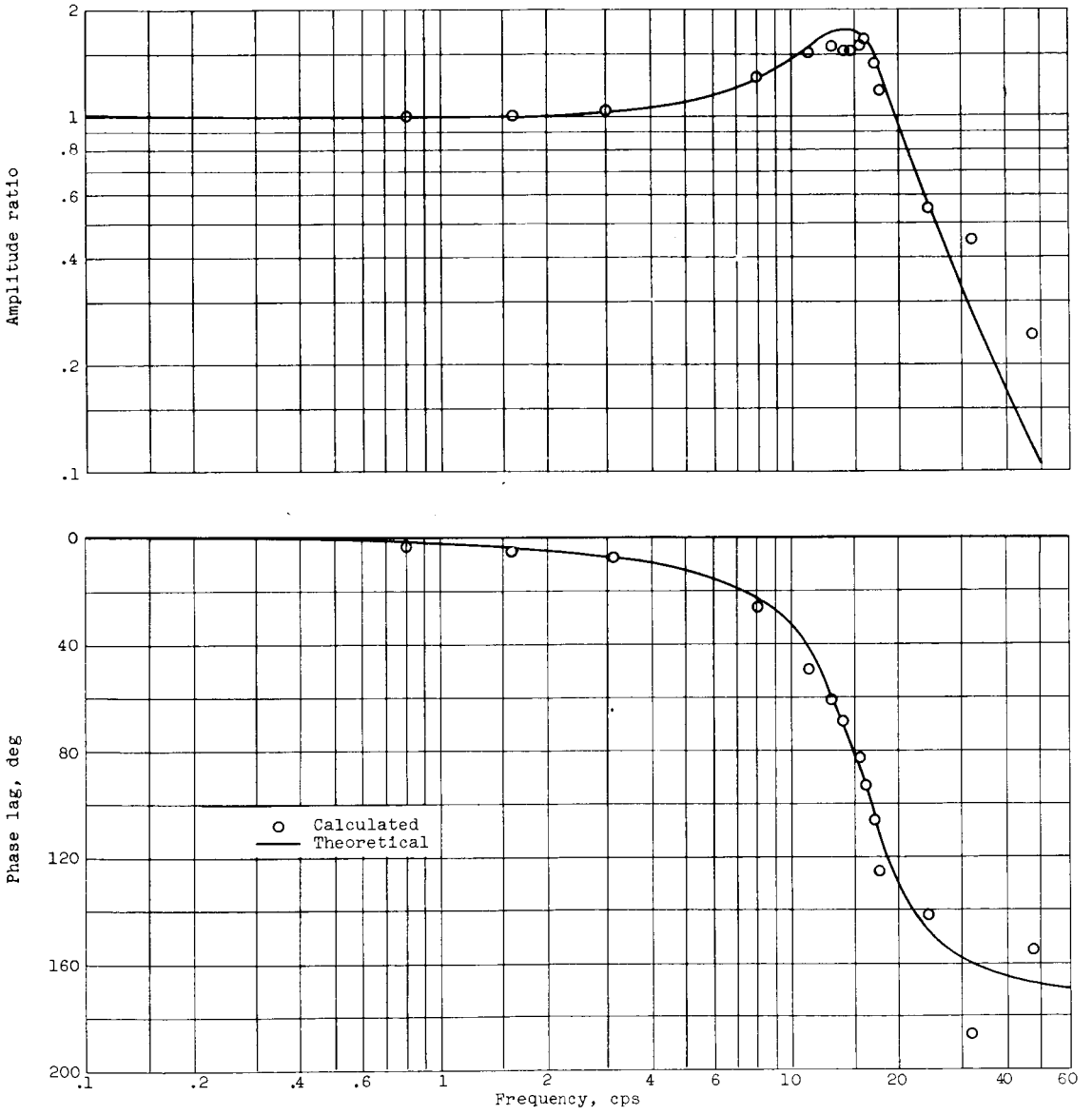

Figure 6. - Frequency response of fuel ΔP pickup and connecting lines (G_{14}).

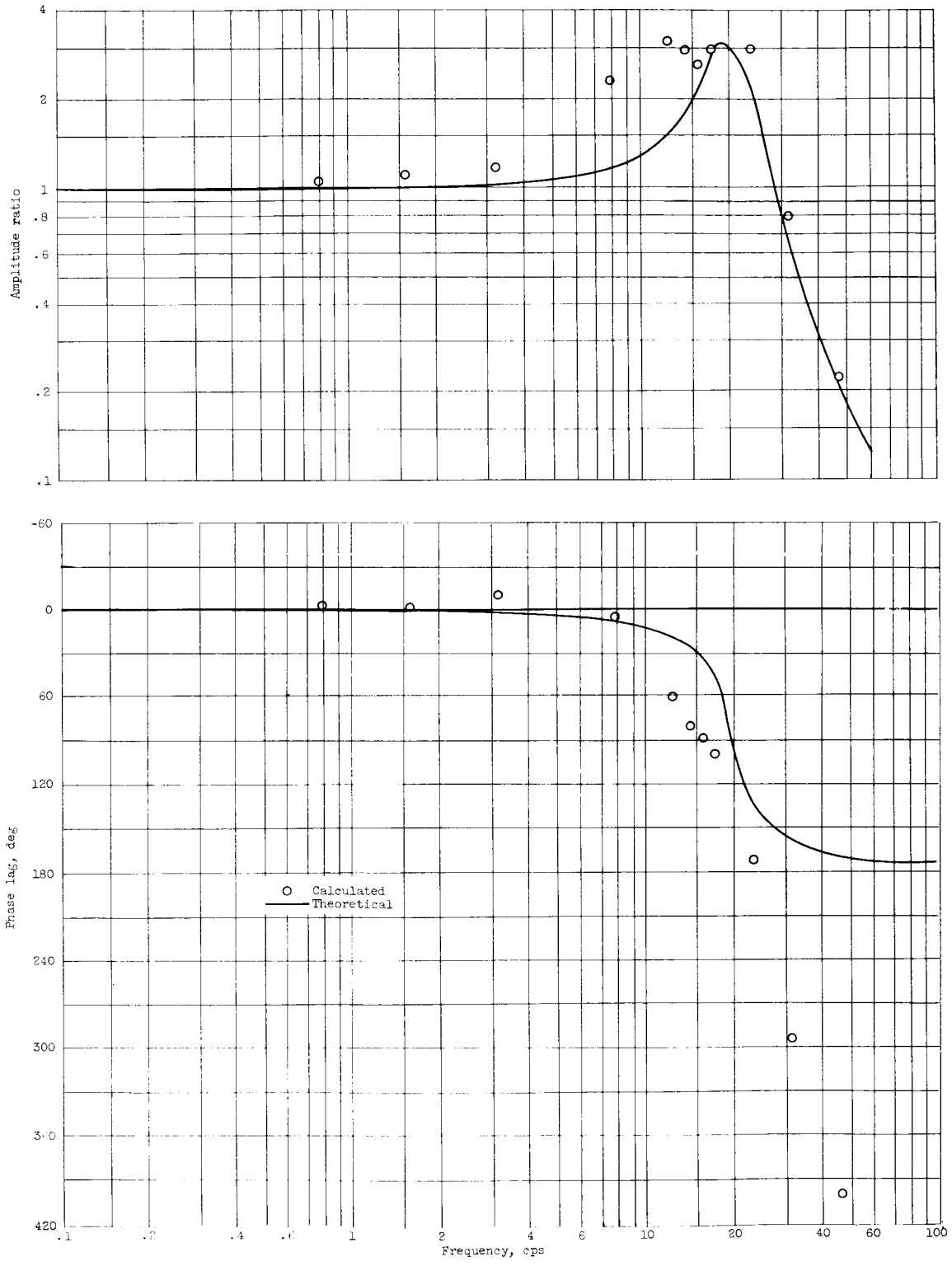

Figure 7. - Frequency response of oxidant ΔP pickup and connecting lines (G_4).

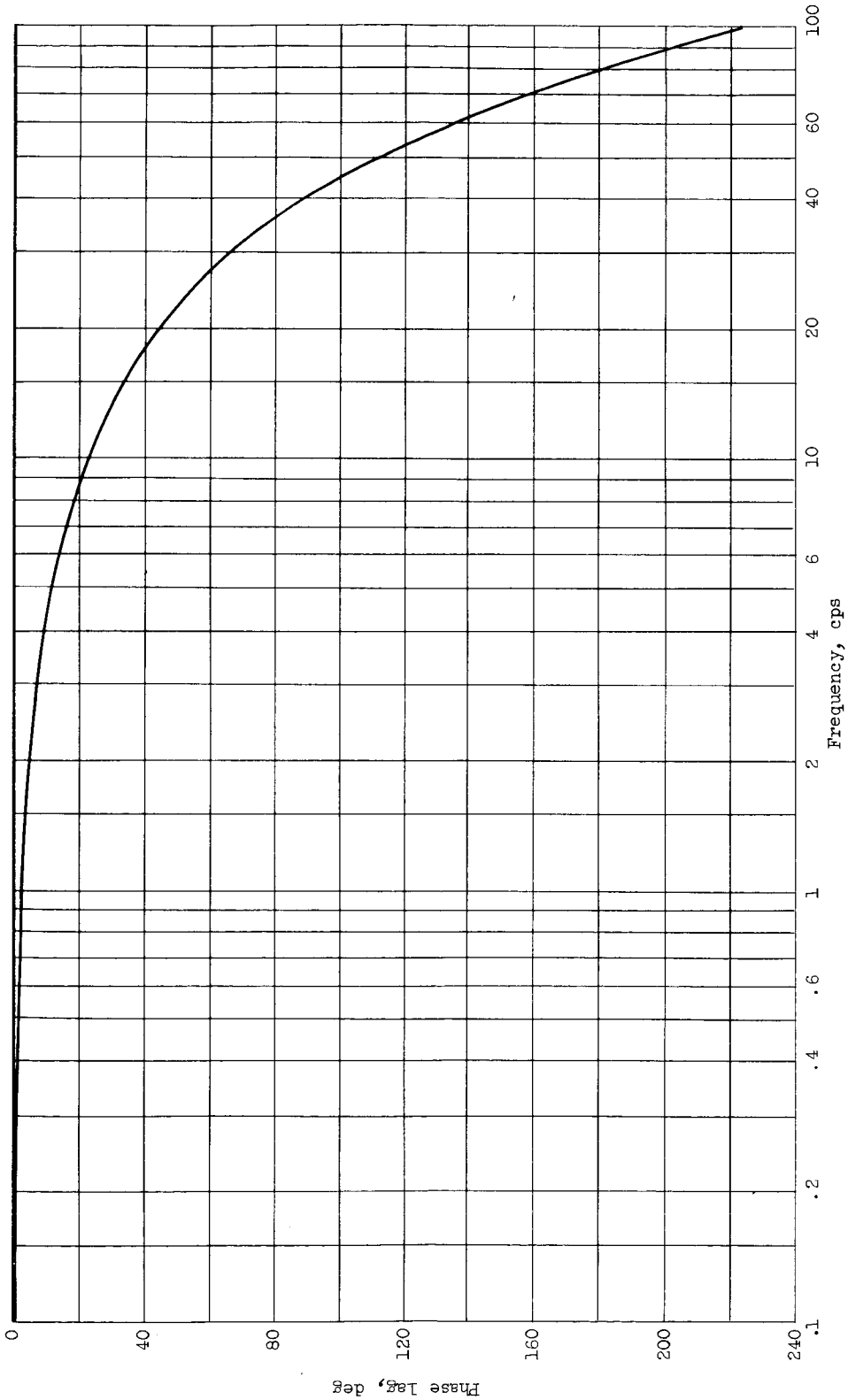

Figure 8. - Relation between phase lag and frequency for dead time of 0.0062 second (e^{-as}).

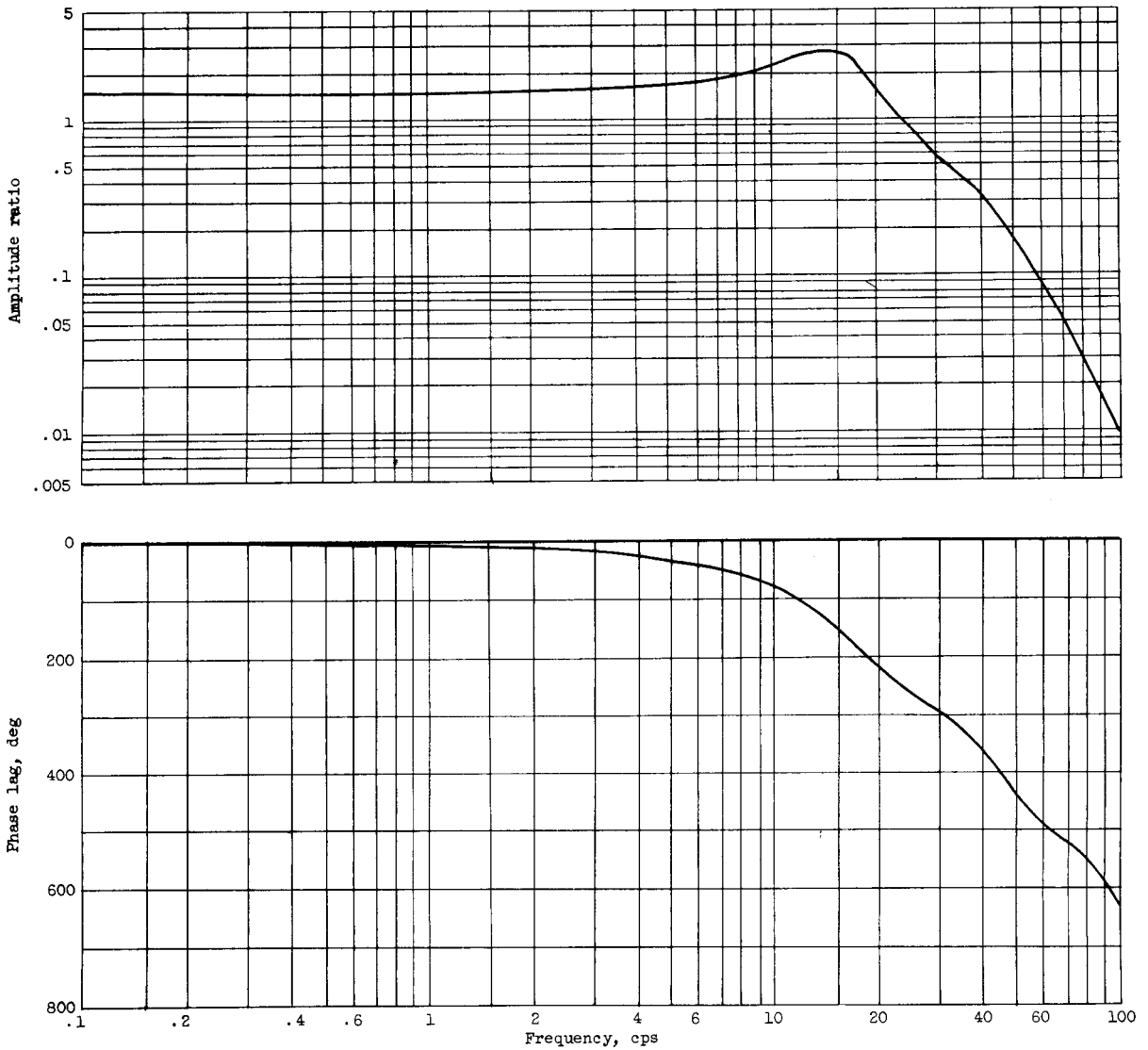

Figure 9. - Open-loop frequency response of fuel control loop ($K_{11}G_{11}K_{12}K_{13}K_{14}G_{14}e^{-as}$).

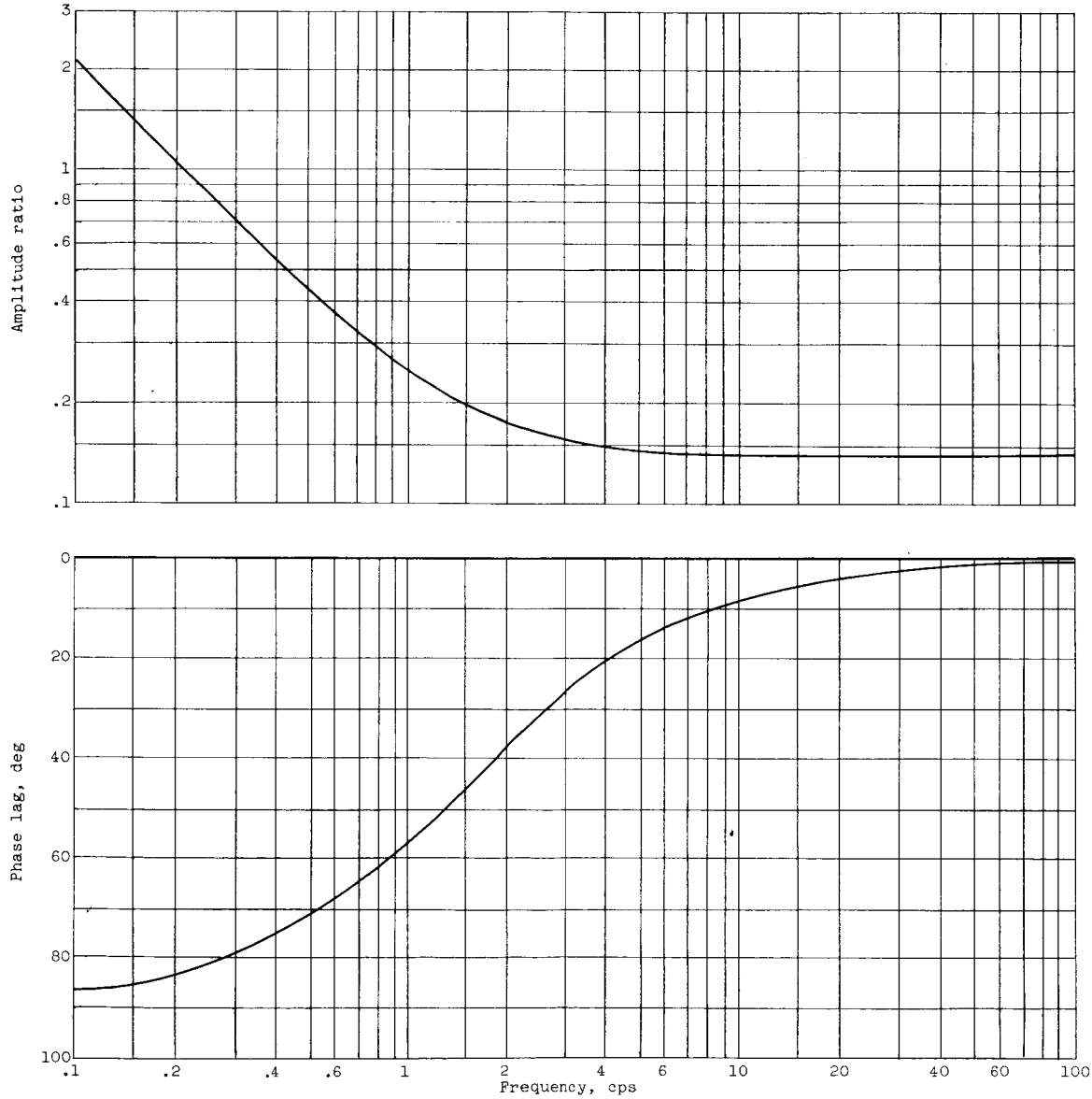

Figure 10. - Frequency response of proportional-plus-integral controller for fuel loop (G_{10}).

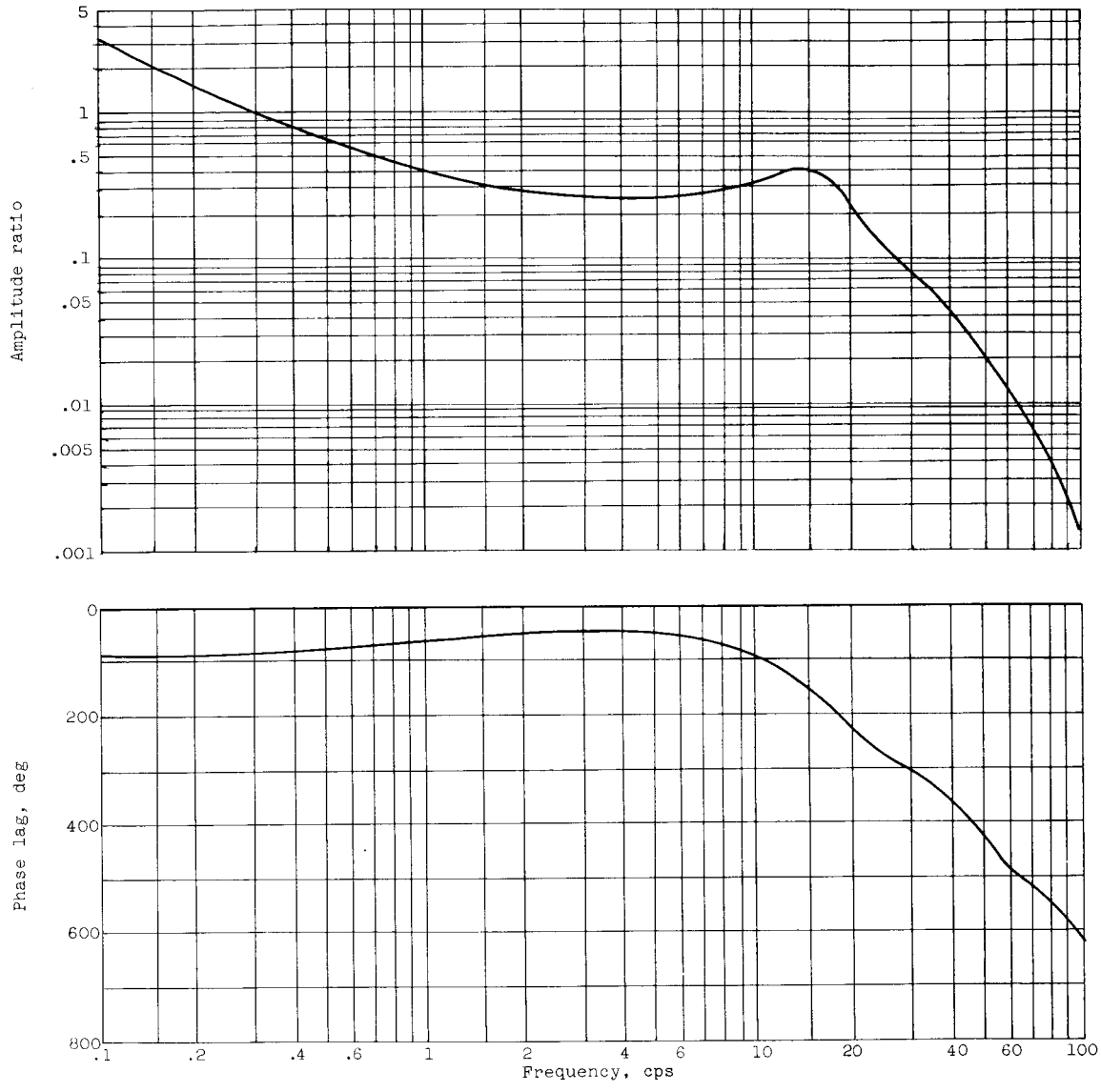

Figure 11. - Open-loop frequency response of fuel control loop with controller ($G_{10}K_{11}G_{11}K_{12}K_{13}K_{14}G_{14}e^{-as}$).

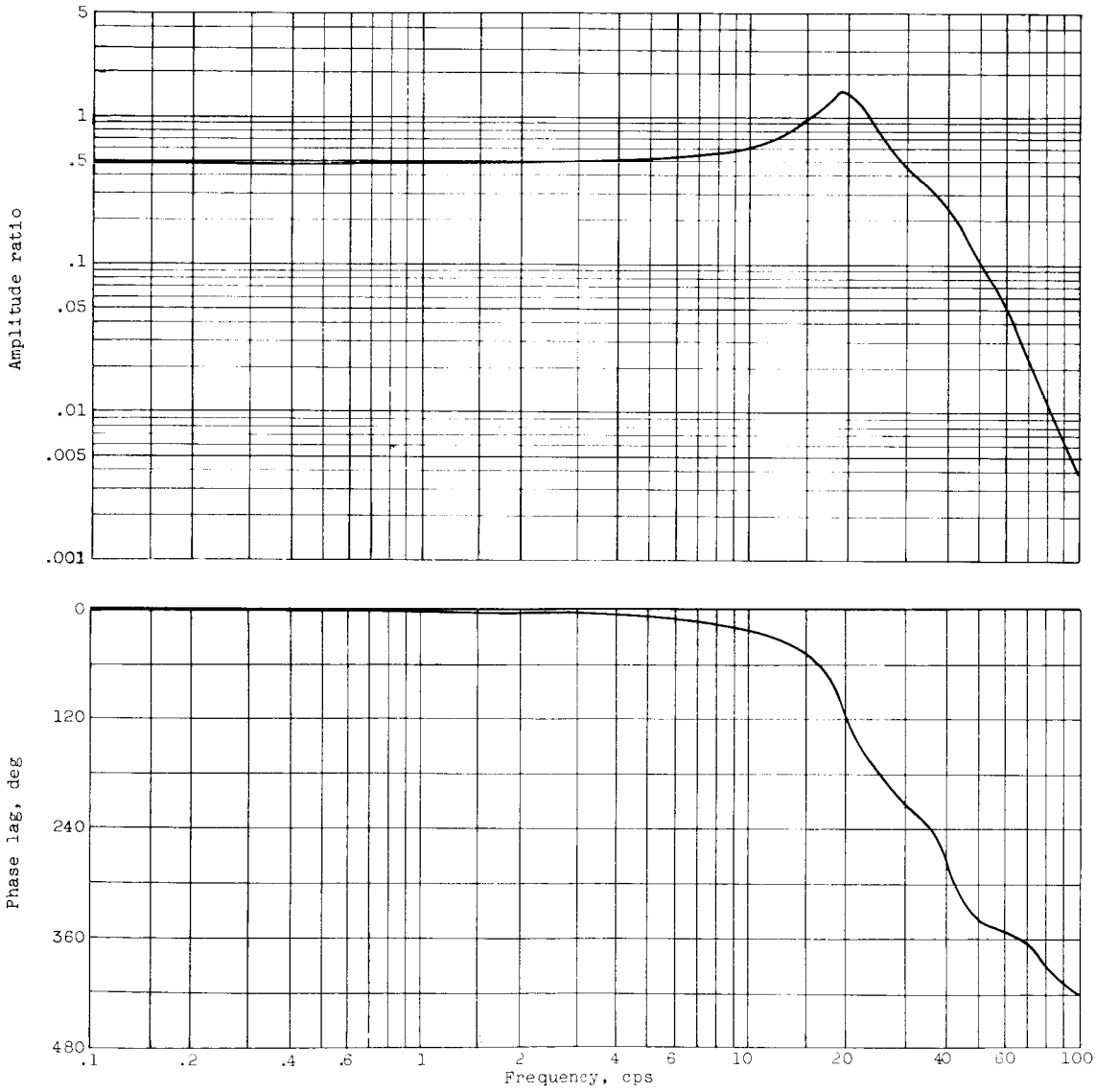

Figure 12. - Open-loop frequency response of oxidant control loop ($K_i G_1 K_2 K_3 K_4 G_4 K_o$).

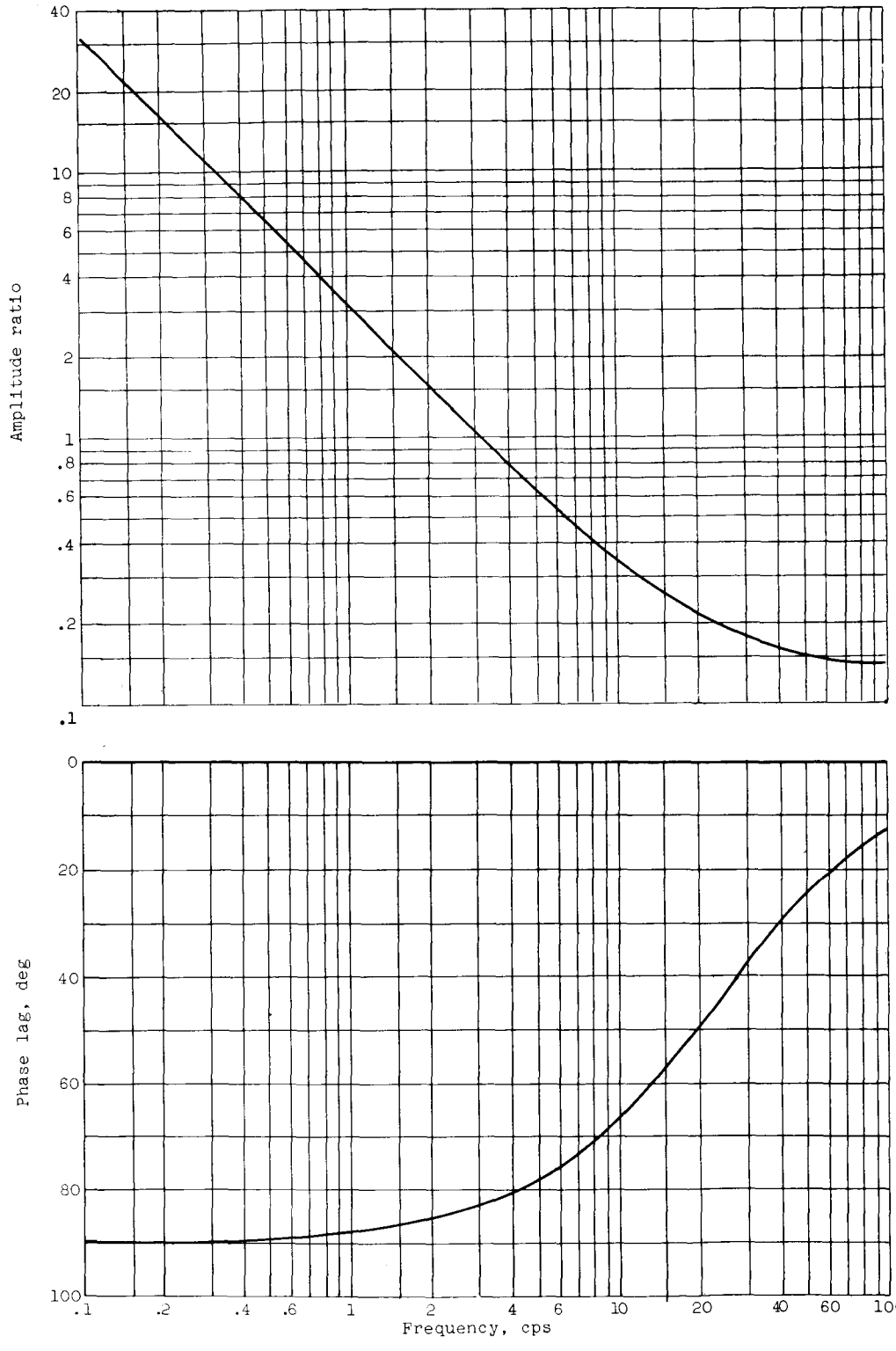

Figure 13. - Frequency response of proportional-plus-integral controller for oxidant control loop (G_O).

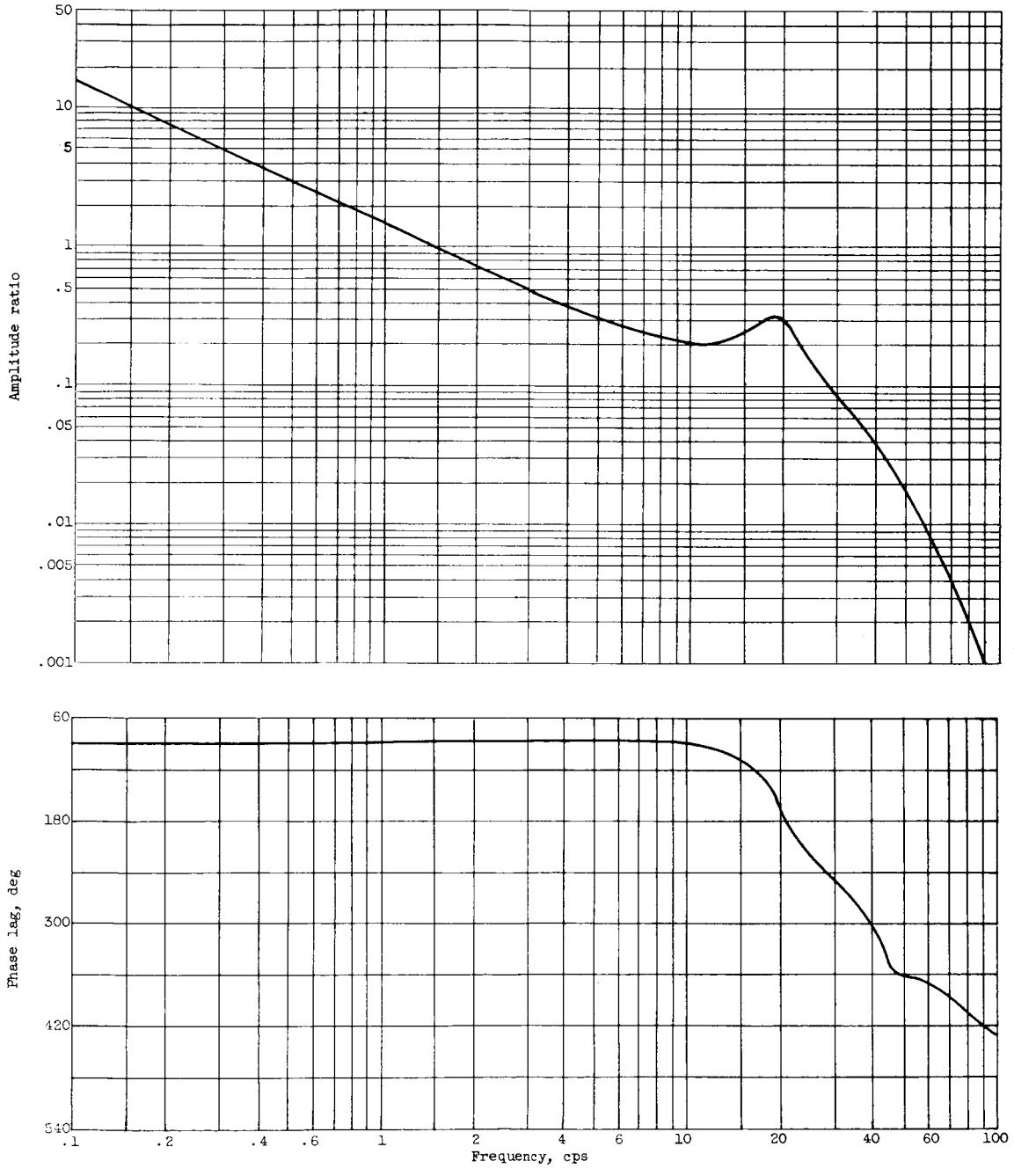

Figure 14. - Open-loop frequency response of oxidant control loop with controller ($G_0K_1G_1K_2K_3K_4G_4K_o$).

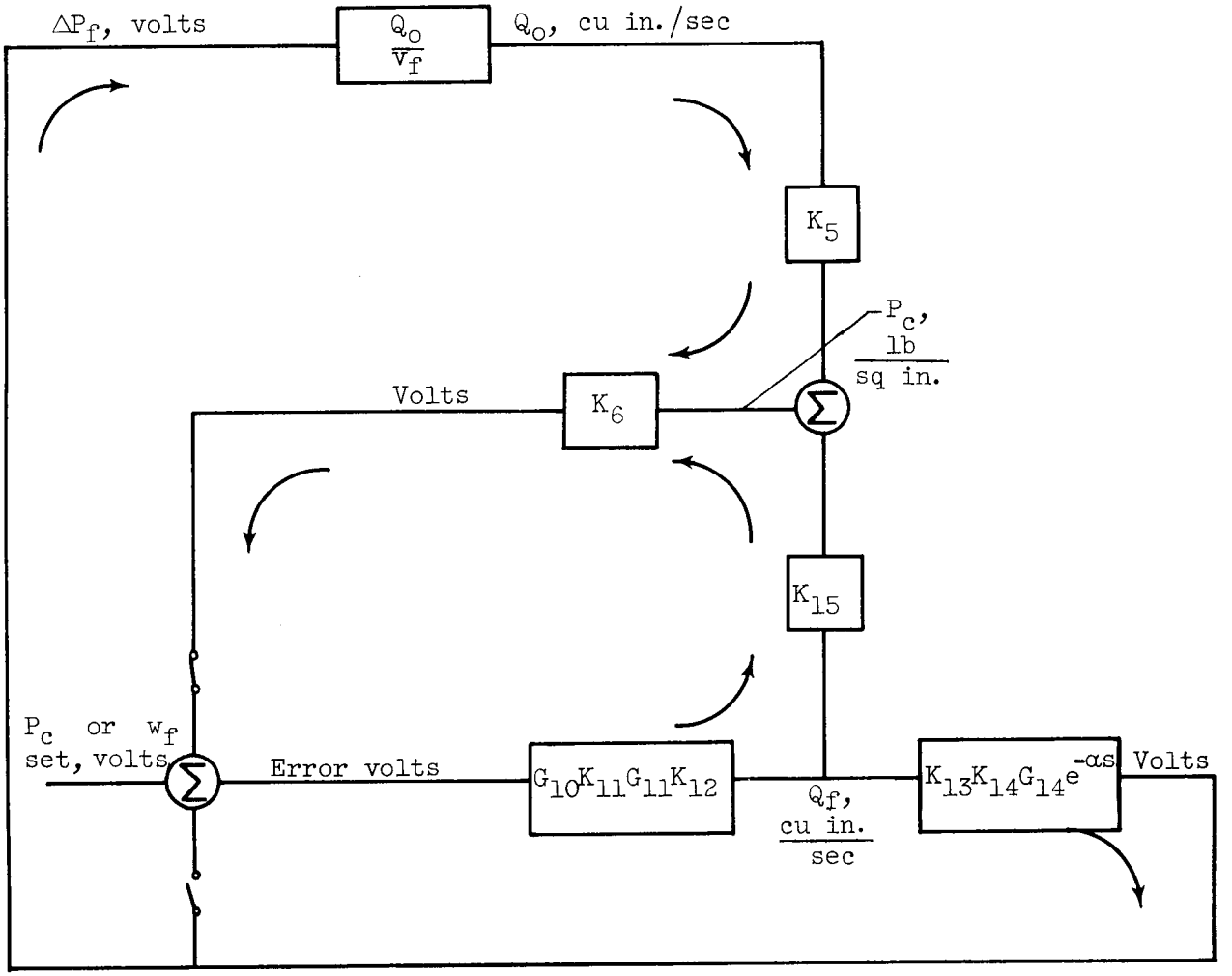

Figure 15. - Block diagram of chamber-pressure and oxidant-fuel-ratio control system reduced to simpler form.

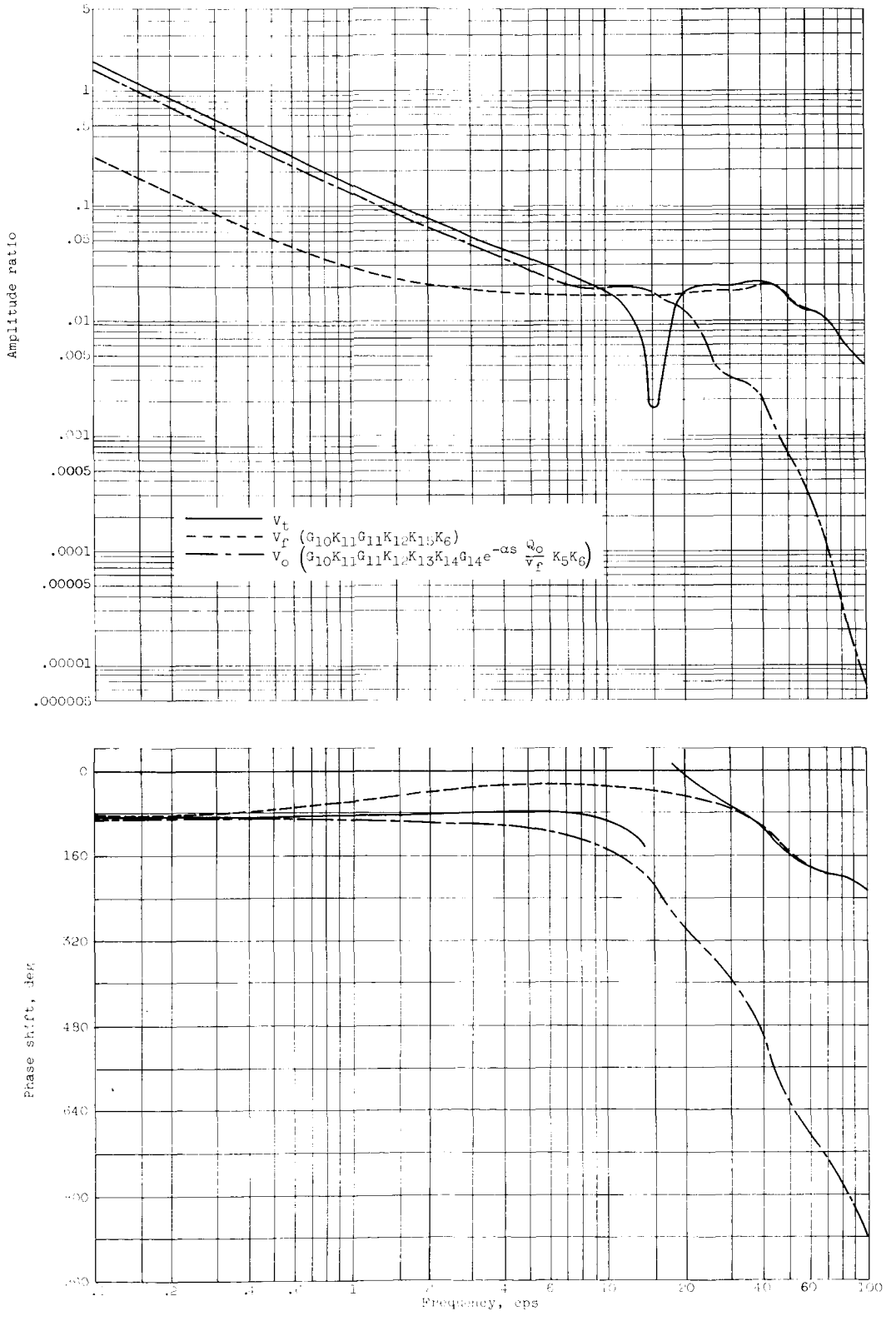

Figure 17. - Feedback frequency response of chamber-pressure control system.

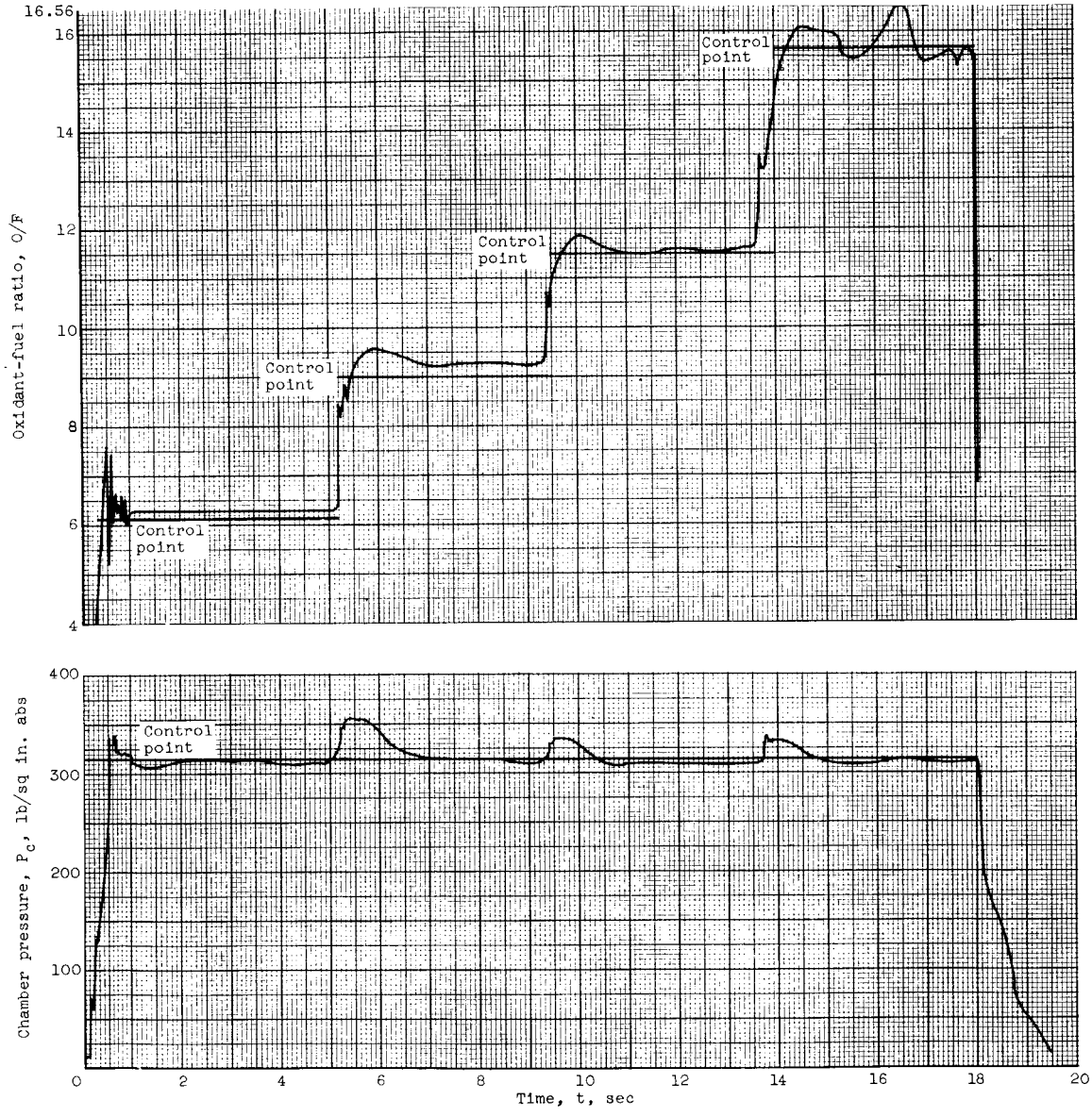

Figure 17. - Time history of run with constant chamber pressure and variable oxidant-fuel ratio.

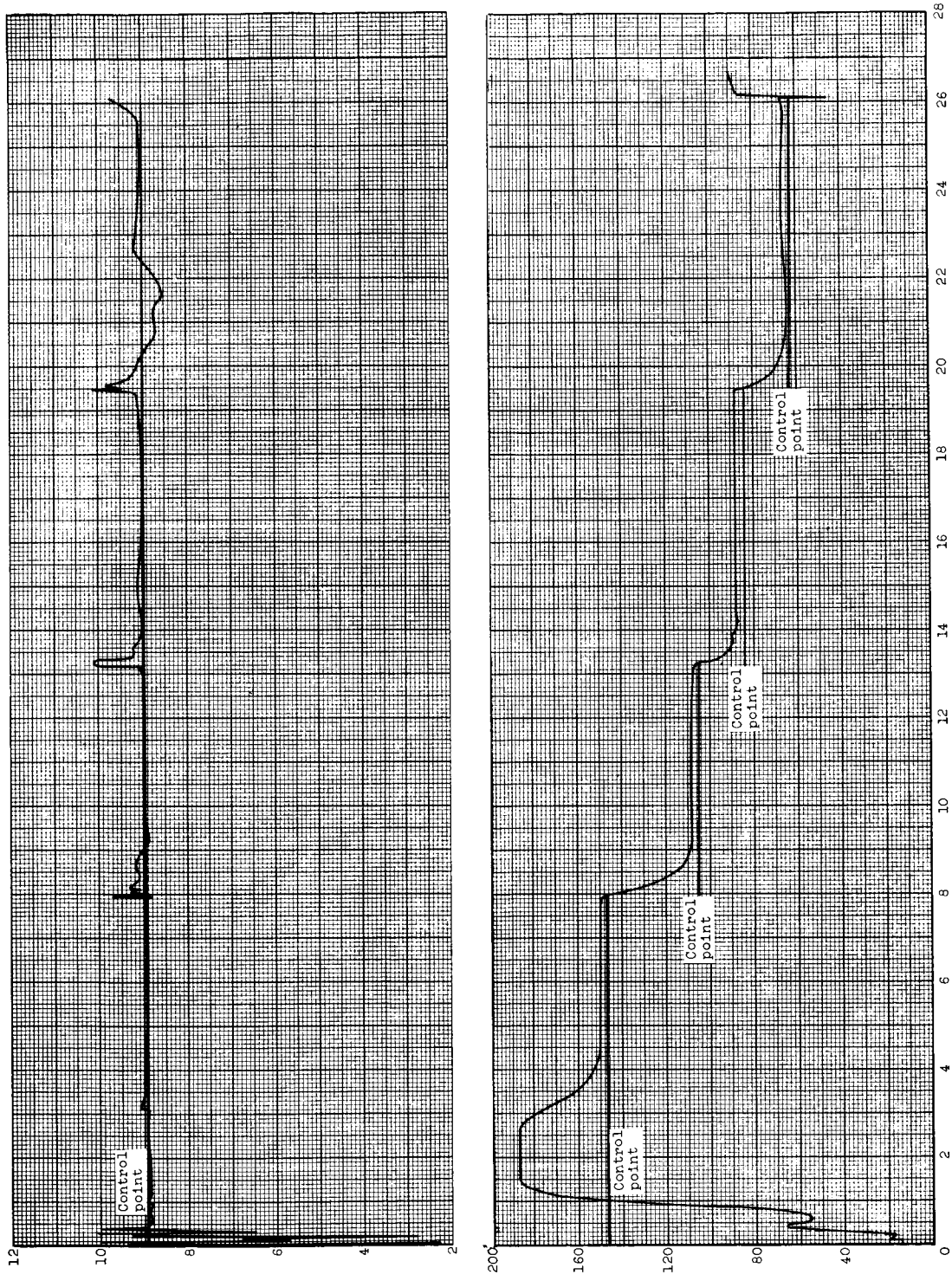

Figure 18. - Time history of run with variable chamber pressure and constant oxidant-fuel ratio of 9.0.

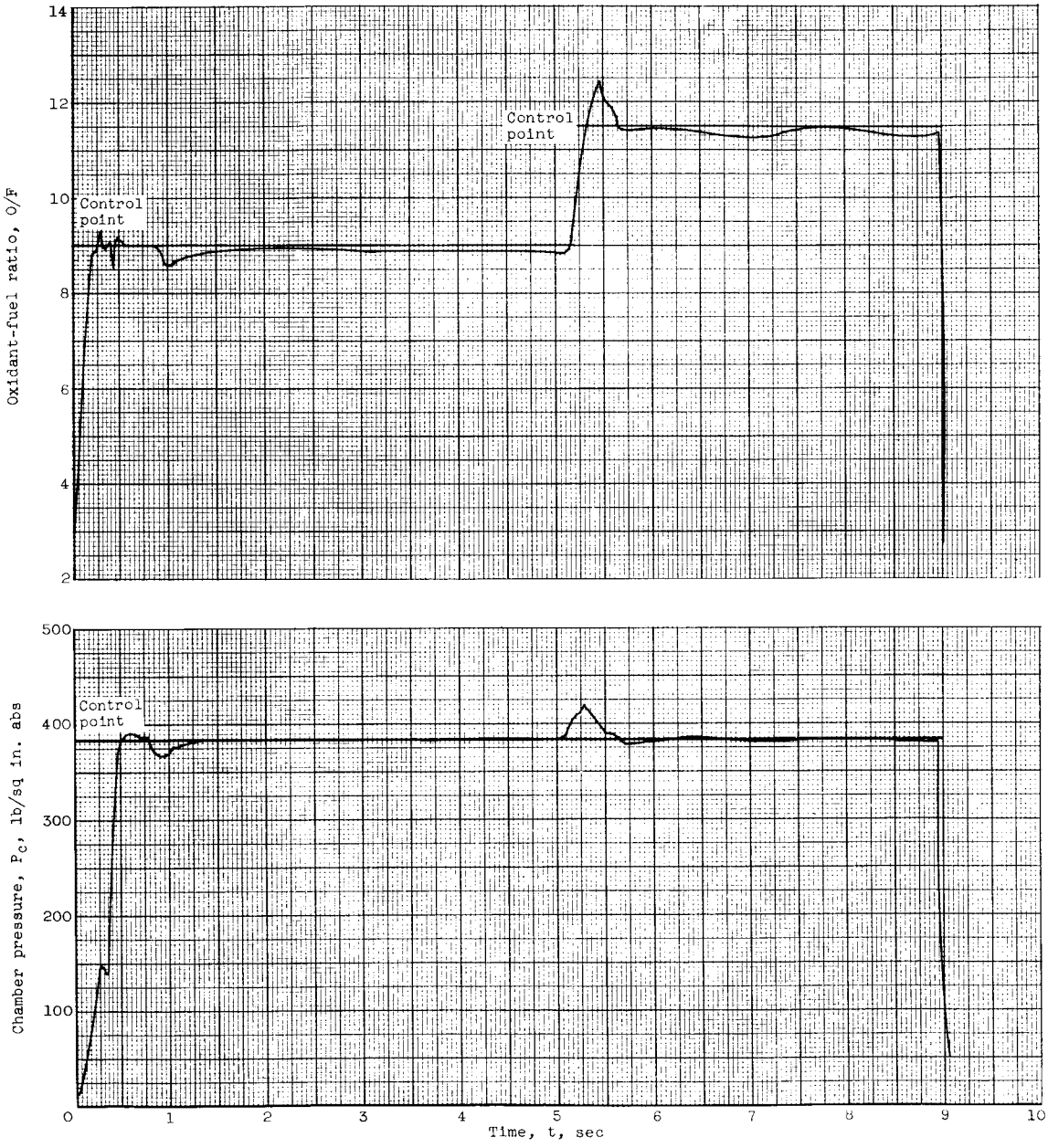

Figure 19. - Time history of run with constant chamber pressure and variable oxidant-fuel ratio (9.0 and 11.5) using chamber-pressure time delay of 0.5 second.

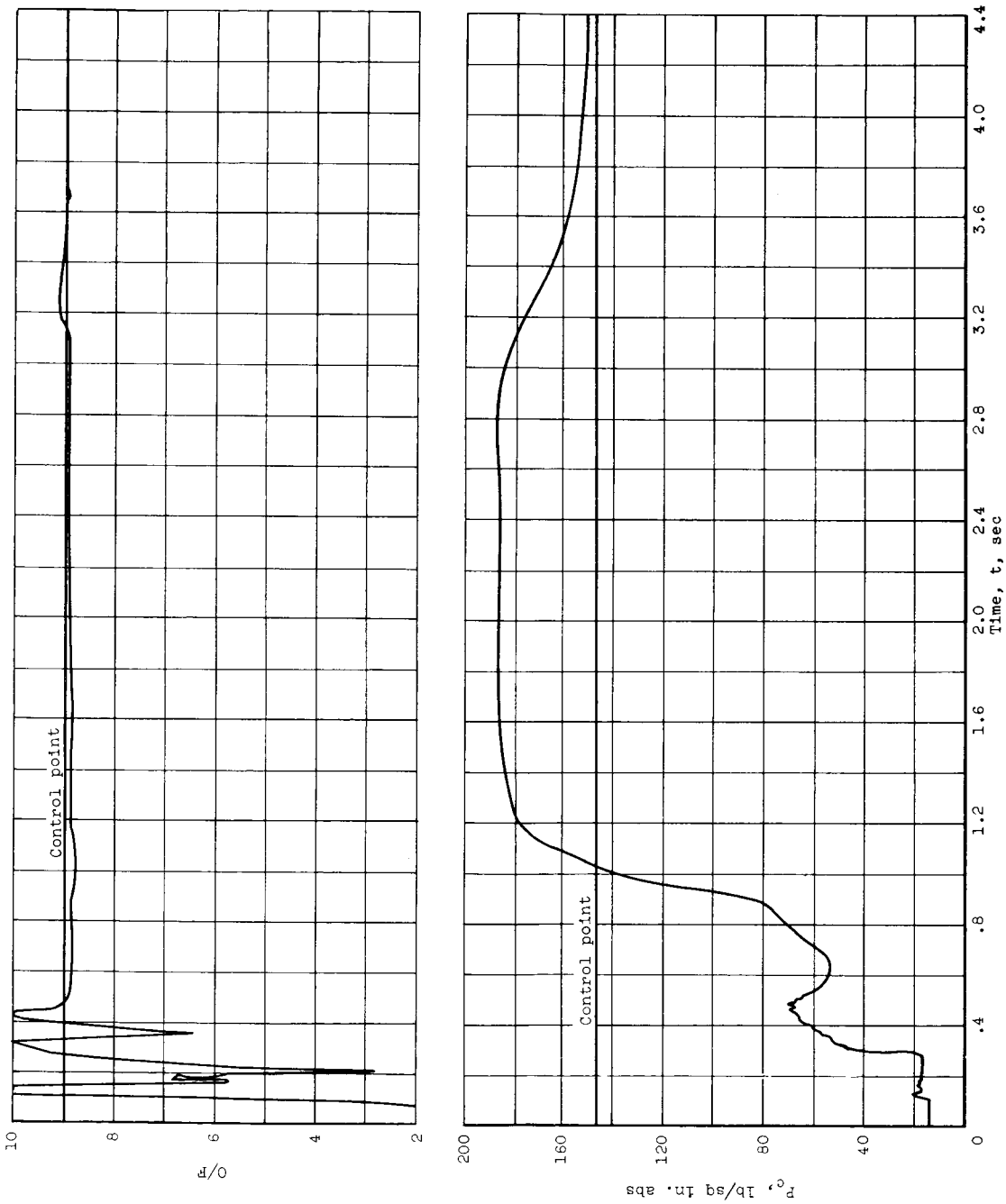

Figure 20. - Time history of startup of run presented in figure 18.

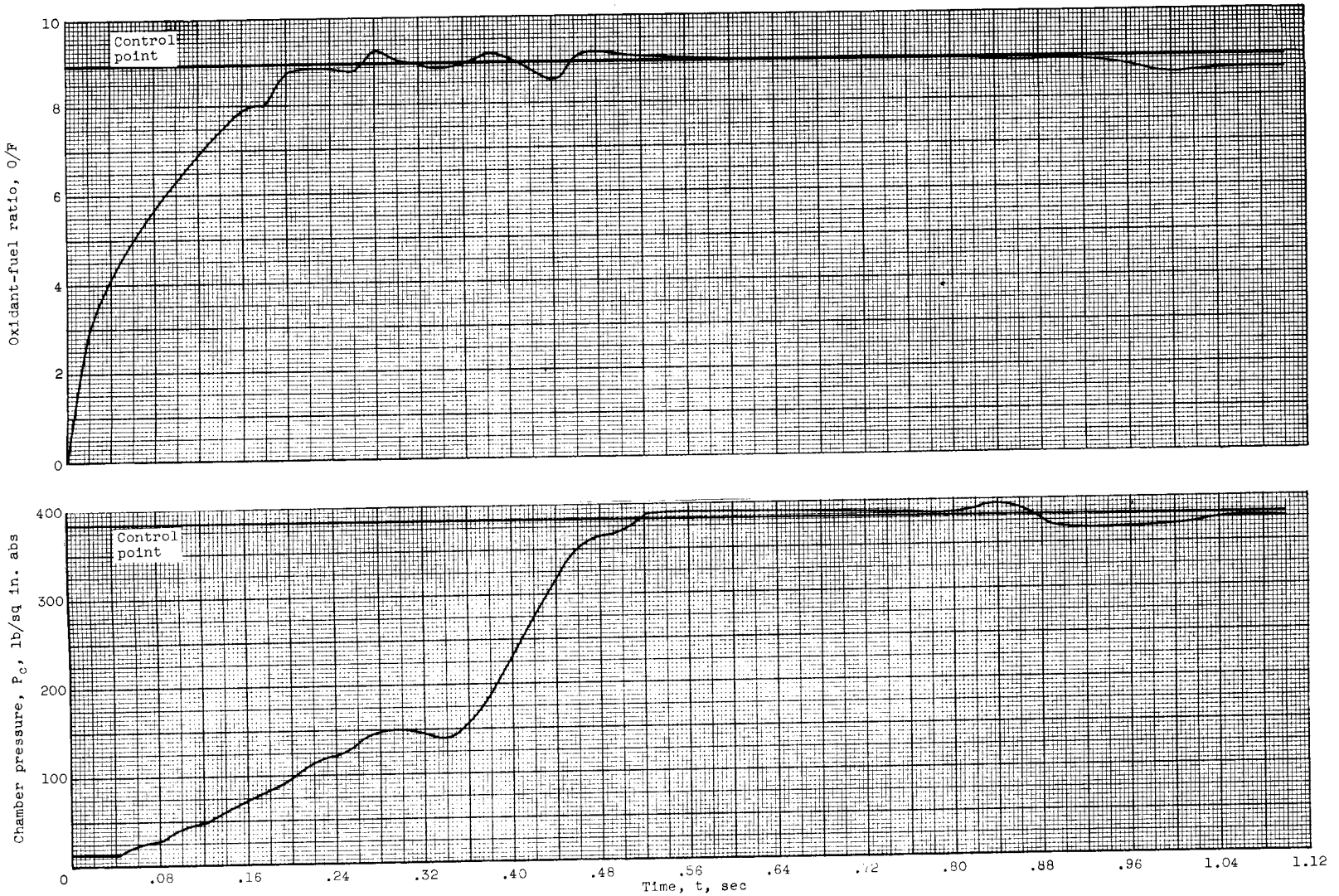

Figure 21. - Time history of startup of run presented in figure 19.

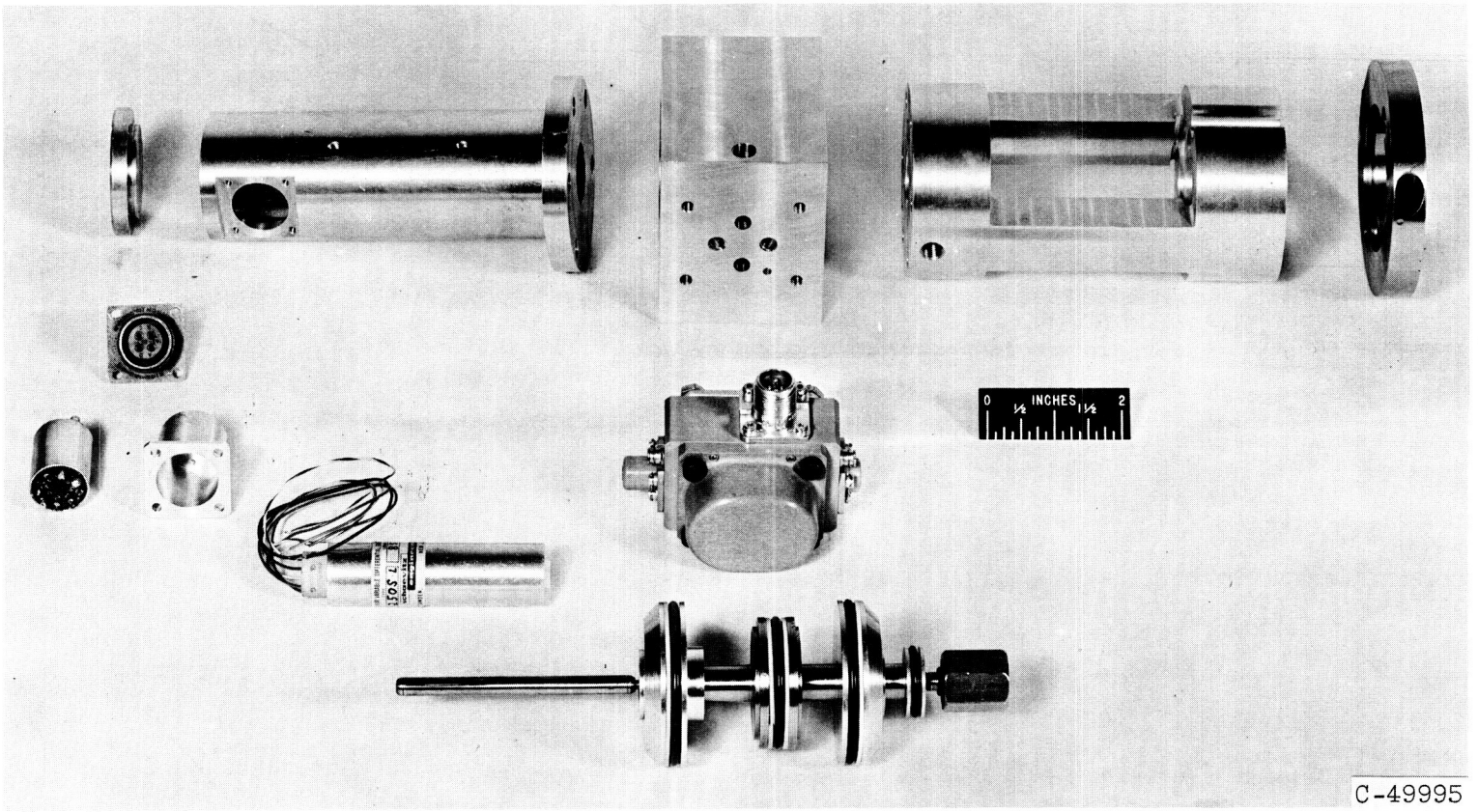

Figure 22. - Disassembled view of electrohydraulic actuator.

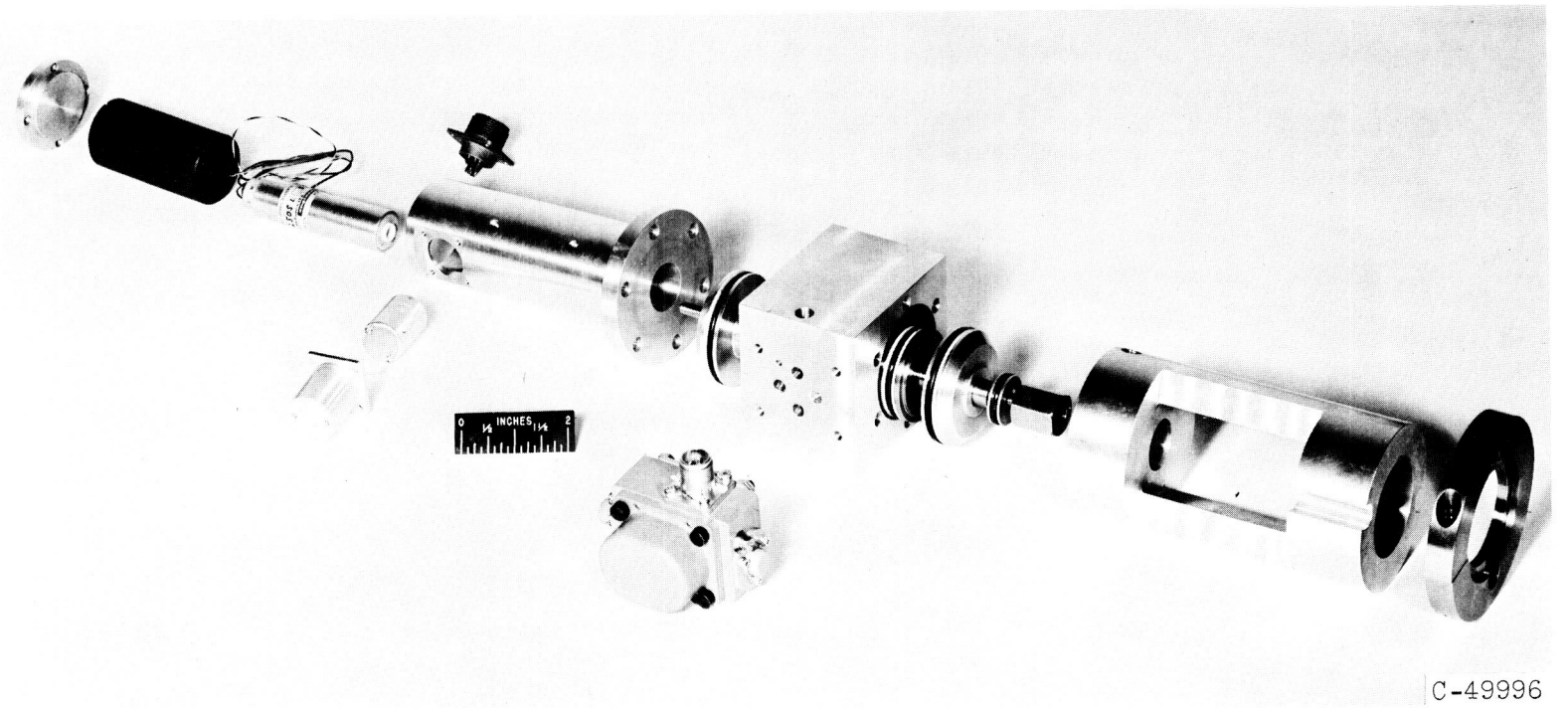

Figure 23. - Exploded view of electrohydraulic actuator.

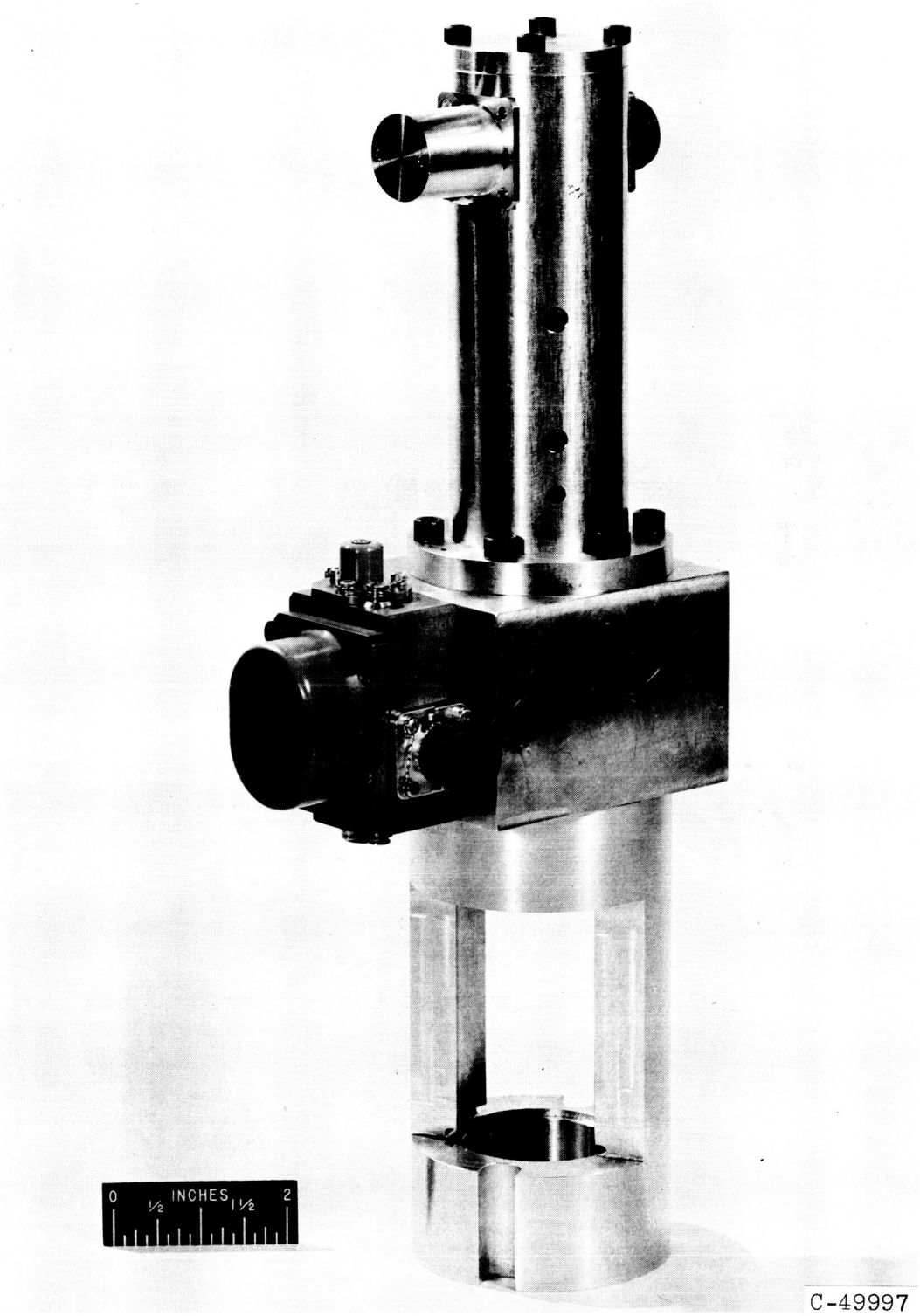

Figure 24. - Assembled electrohydraulic actuator.

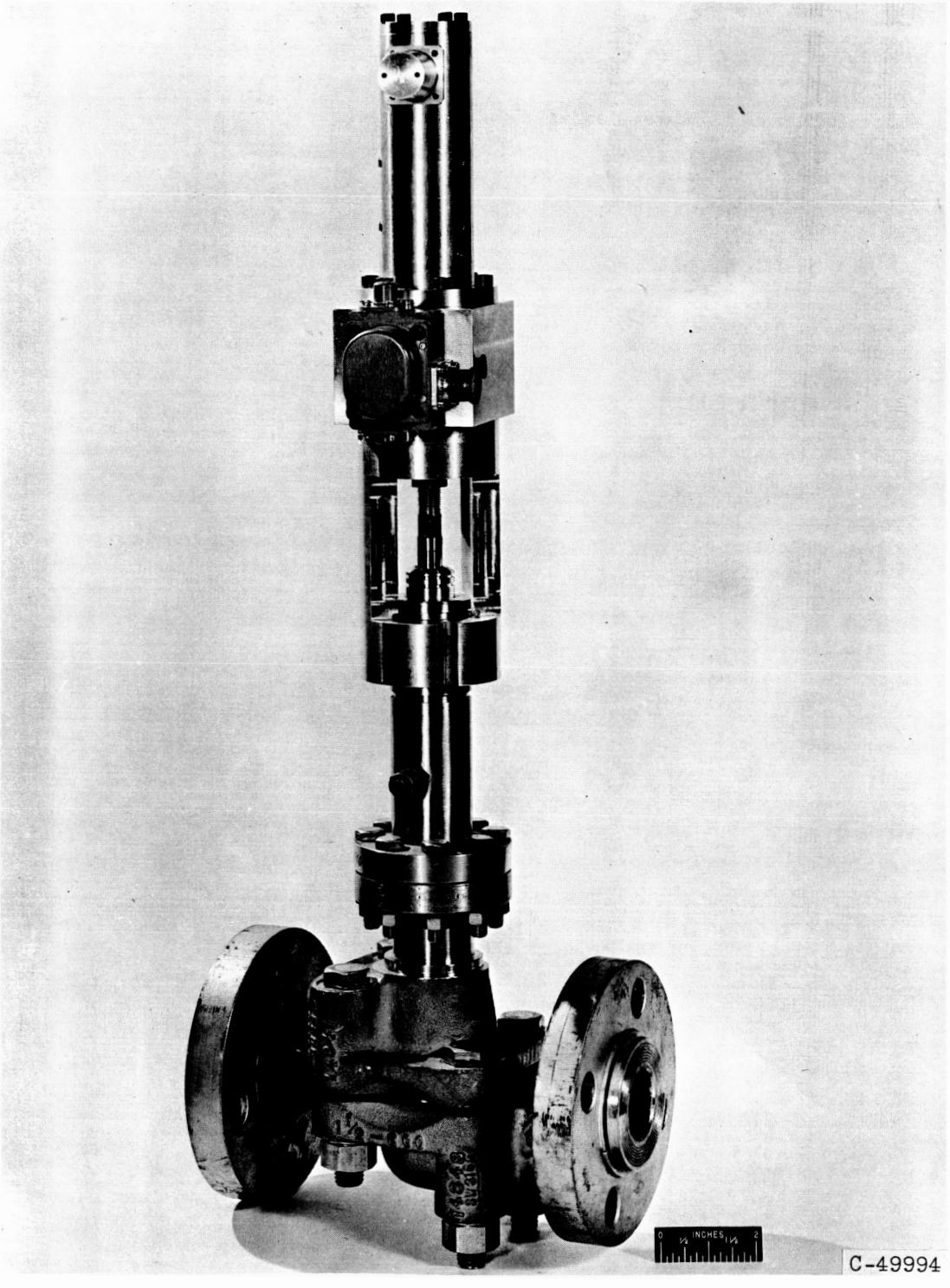

Figure 25. - Mockup of electrohydraulic actuator mounted on control valve.

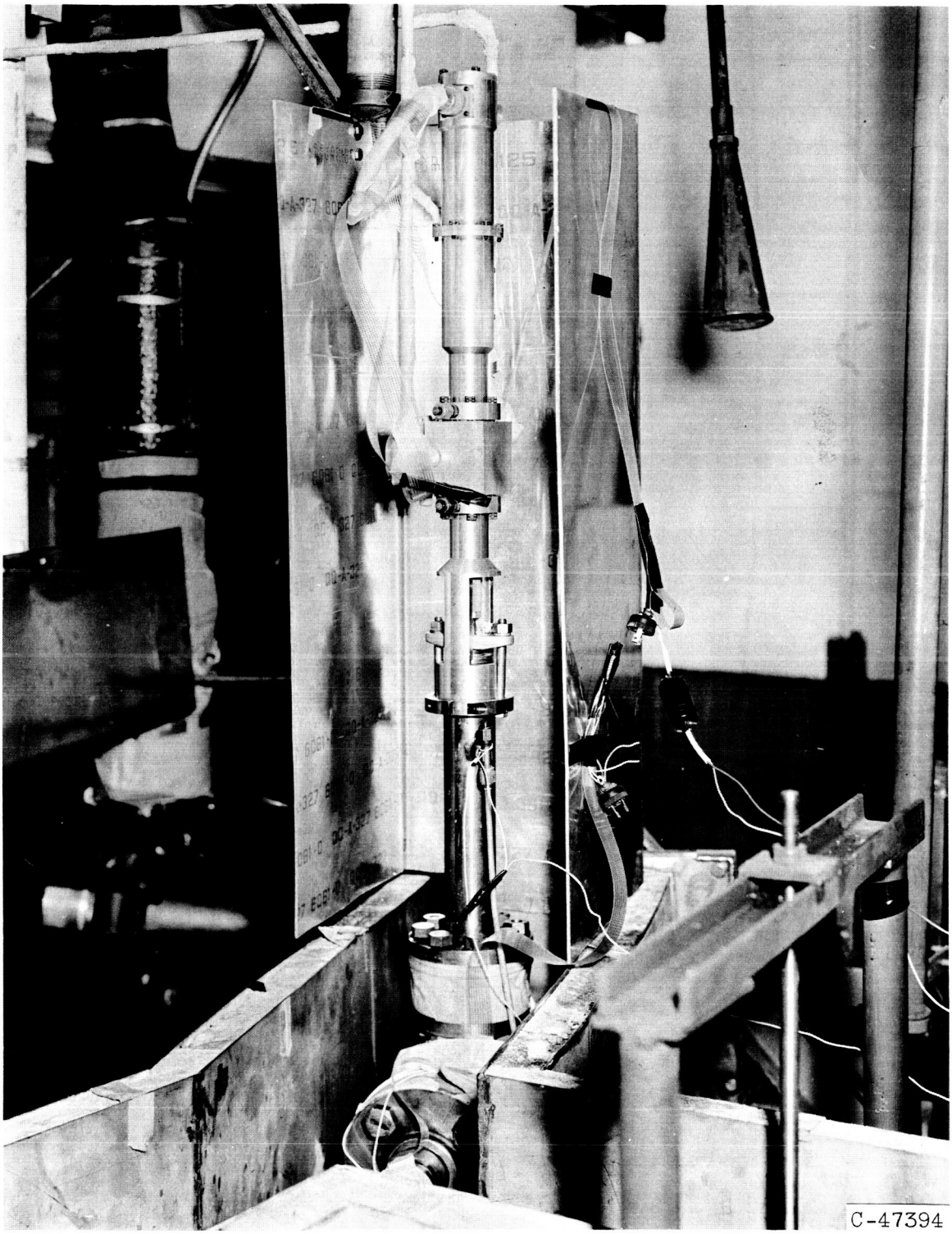

Figure 26. - View of fluorine actuator and control valve installed in test cell.

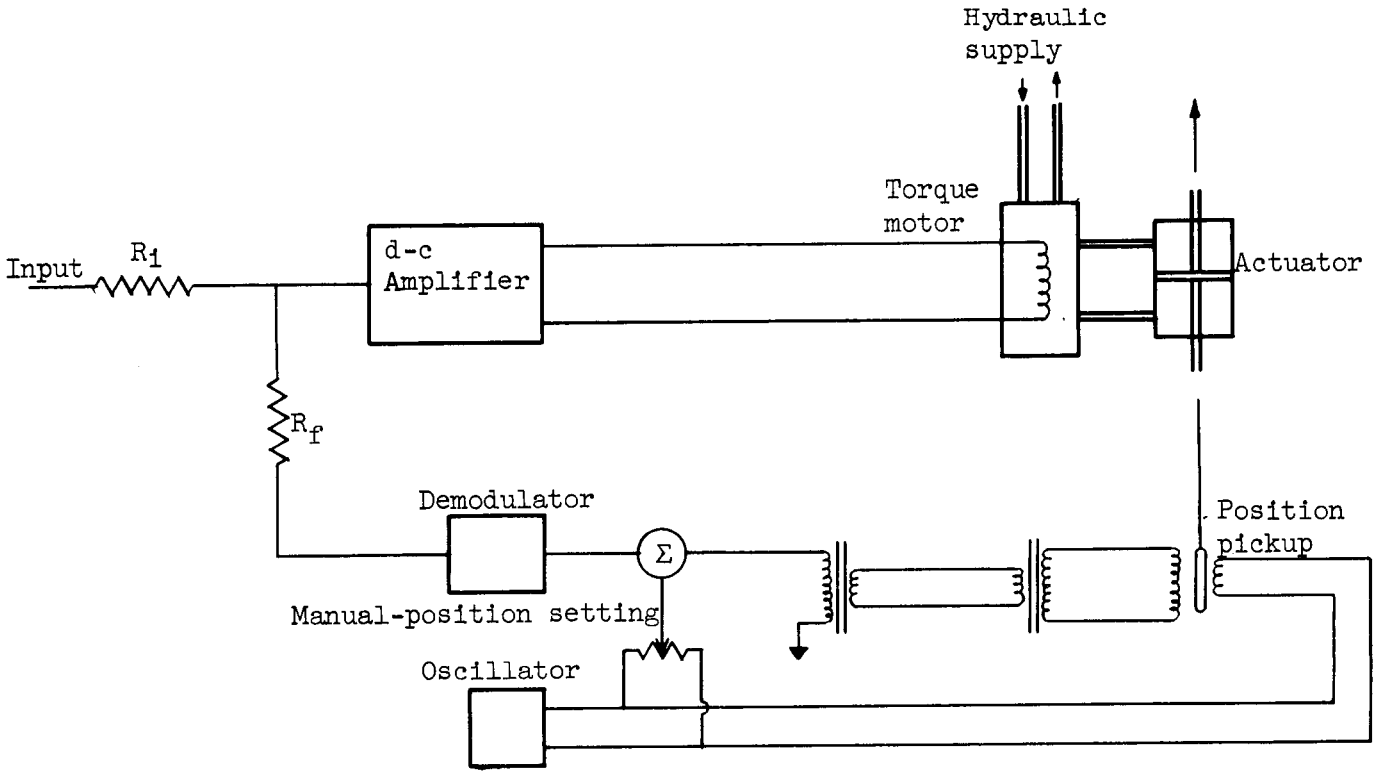

Figure 27. - Schematic diagram of electronic servoamplifier.

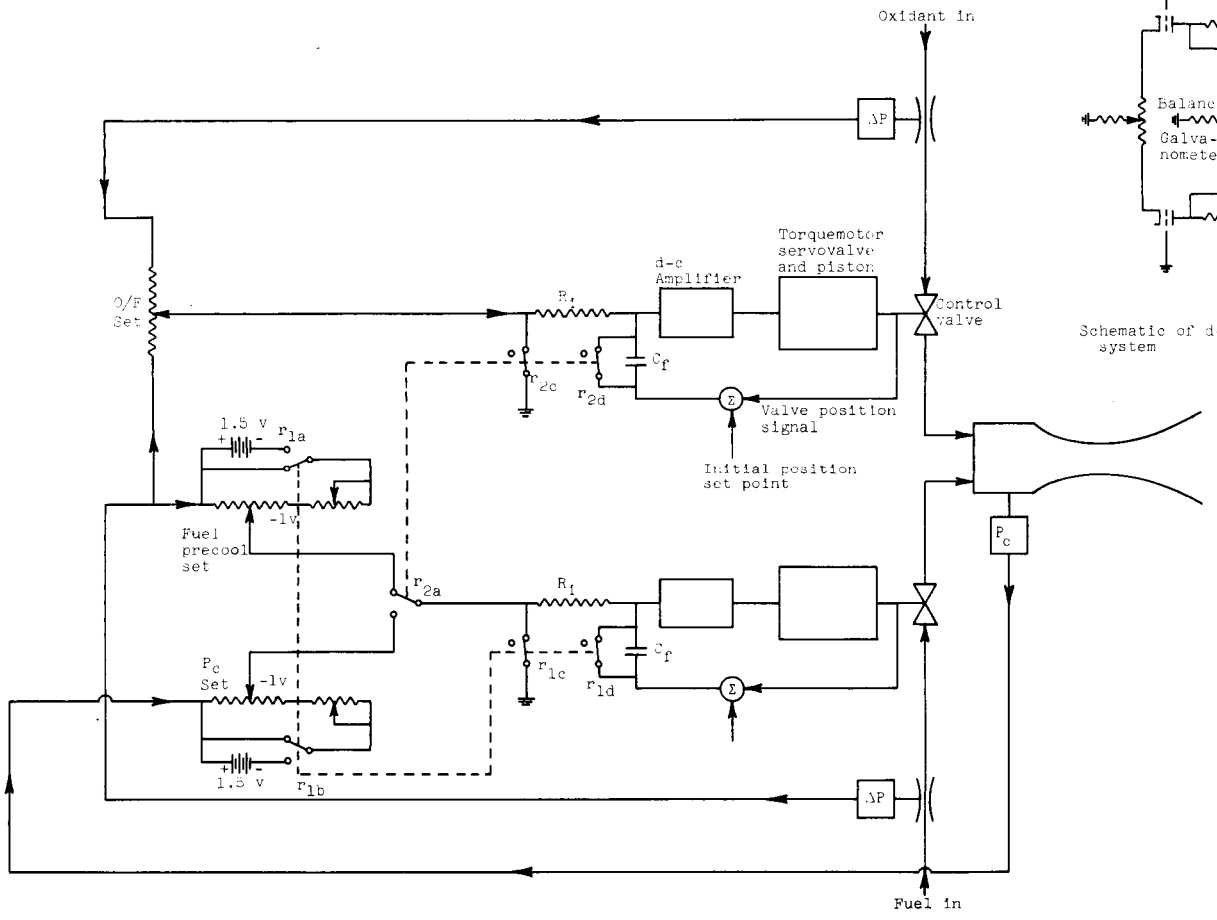

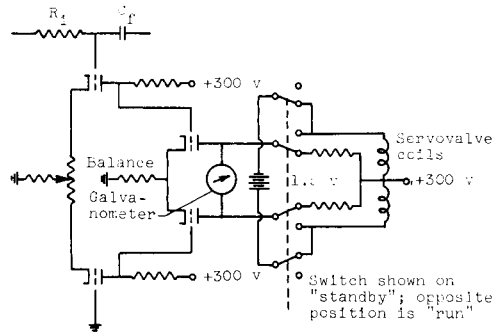

Schematic of d-c amplifier showing balancing system

Figure 28. - Schematic wiring diagram of rocket-engine control system.

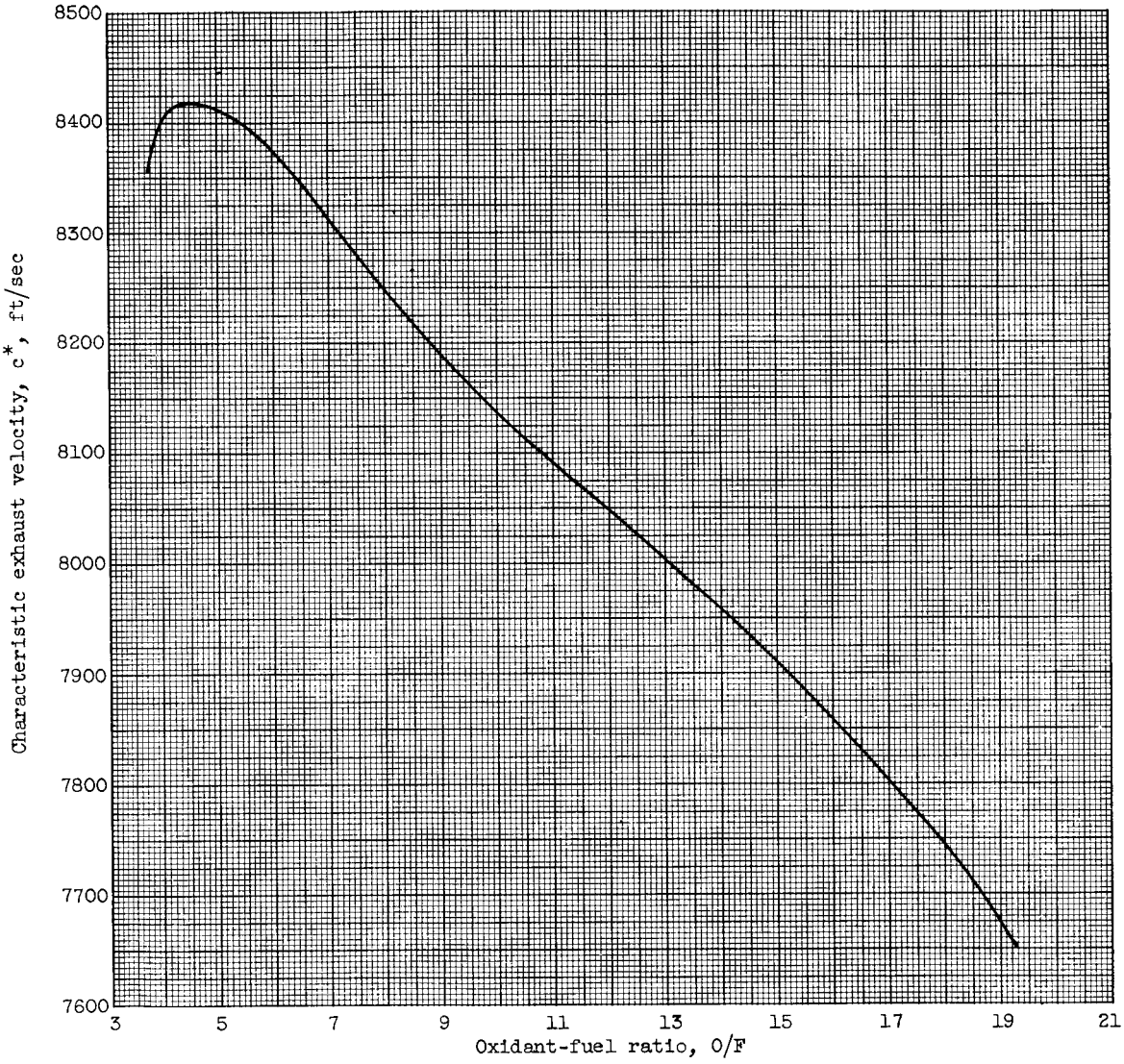

Figure 29. - Variation of characteristic exhaust velocity with oxidant-fuel ratio (theoretical). Chamber pressure, 300 pounds per square inch.

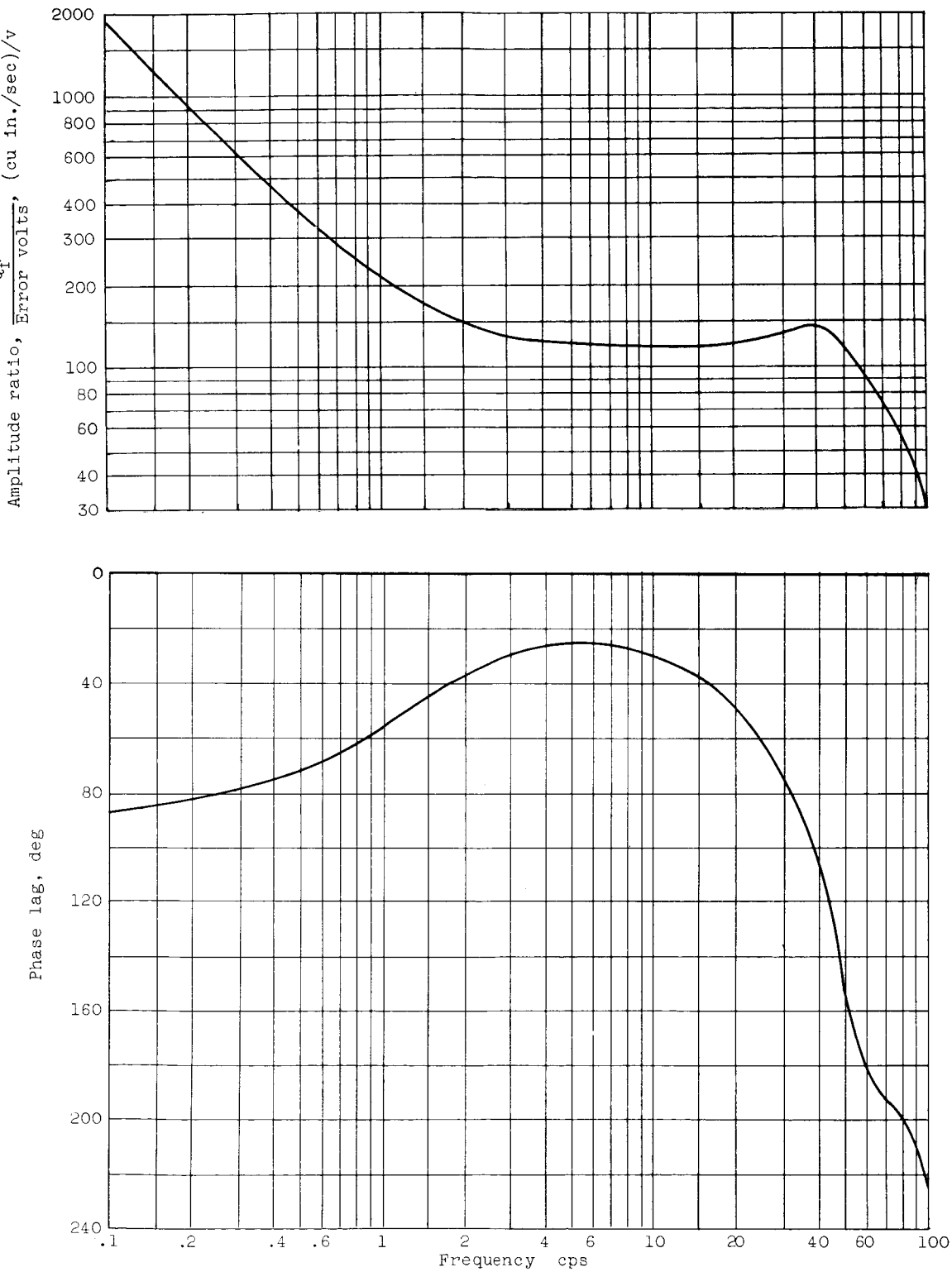

Figure 30. - Frequency response of elements in fuel control forward loop ($G_{10}K_{11}G_{11}K_{12}$).

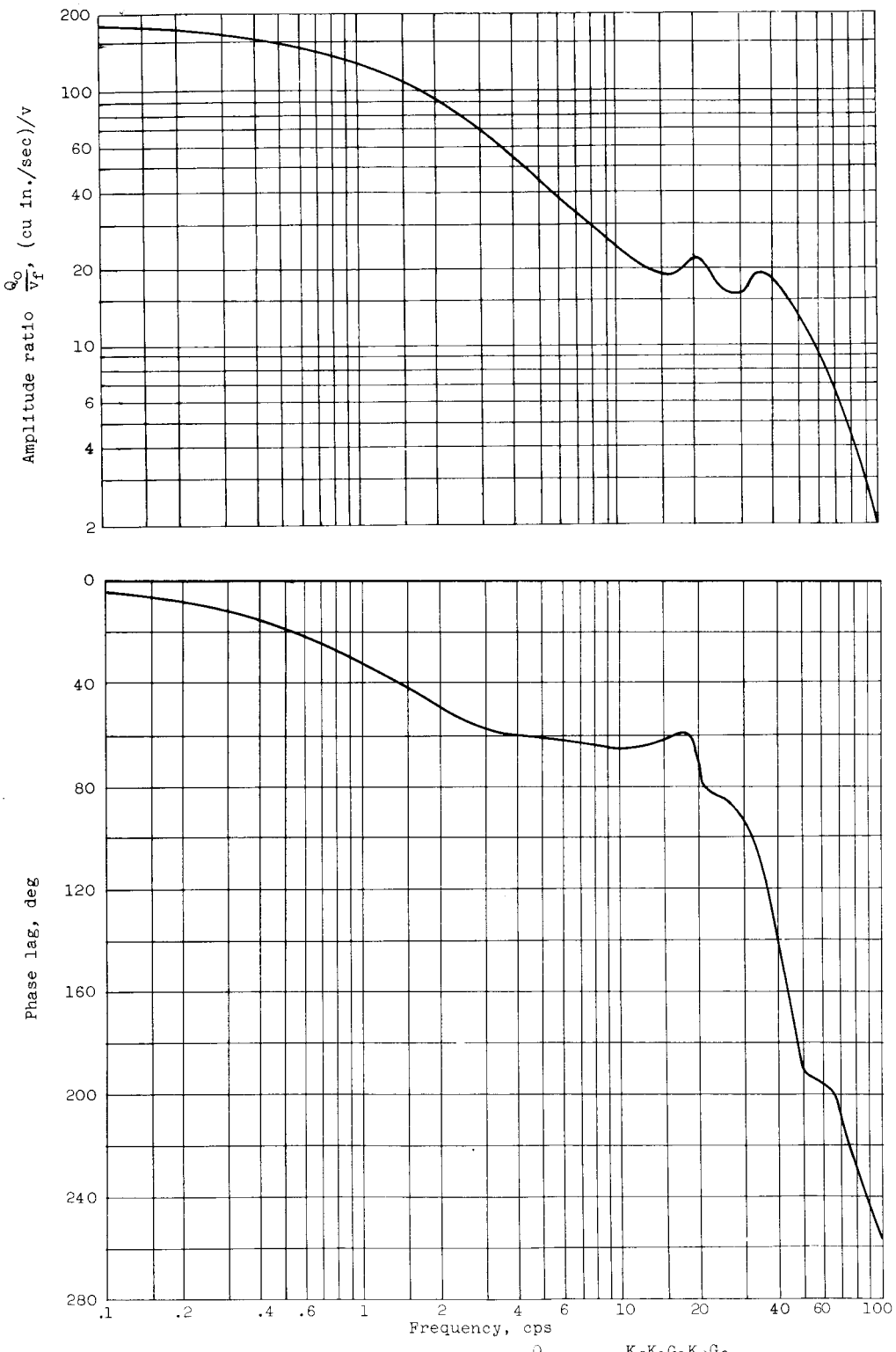

Figure 31. - Frequency response of $\frac{Q_o}{v_f} = \frac{K_f K_1 G_1 K_2 G_o}{1 + K_1 G_1 K_2 K_3 K_4 G_4 K_o G_o}$.

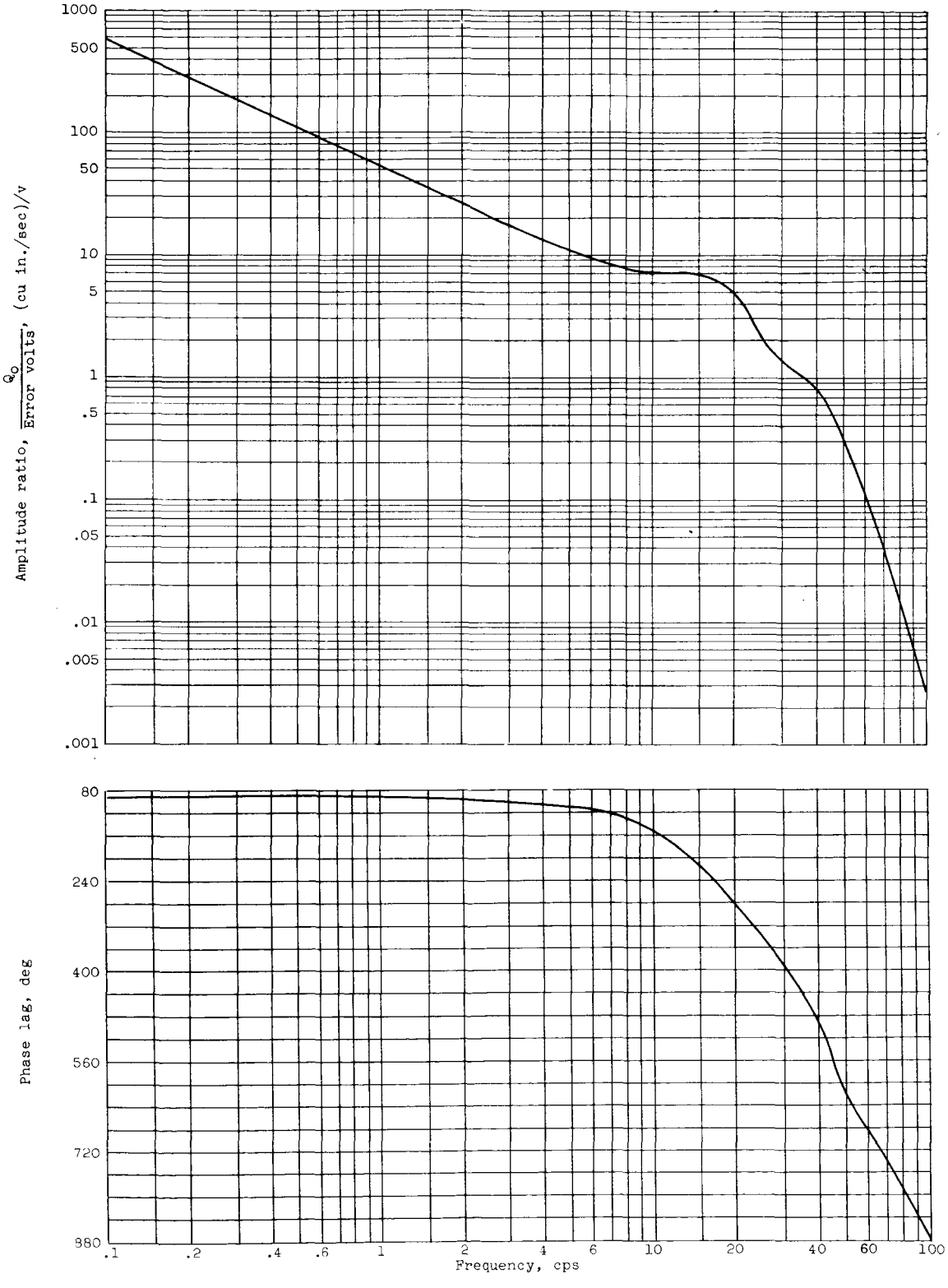

Figure 32. - Frequency response of oxidant flow to error voltage applied to fuel controller G_{10}.